

SOME CONSIDERATIONS IN WIND-TUNNEL

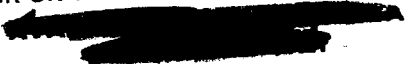
TESTS OF V/STOL MODELS

By Harry H. Heyson

NASA Langley Research Center  
Langley Station, Hampton, Va.

Lecture presented at the University of  
Tennessee Space Institute in a  
Short Course In

Modern Developments in Low Speed Aerodynamics  
With Application to VTOL

FF No. 602(B)	<u>N68-13016</u>	(THRU)
	(ACCESSION NUMBER)	
	<u>60</u>	(CODE)
	(PAGES)	
	<u>TMX-60772</u>	<u>01</u>
	(NASA CR OR TMX OR AD NUMBER)	(CATEGORY)
		

Tullahoma, Tennessee  
September 29, 1967

## SOME CONSIDERATIONS IN WIND-TUNNEL TESTS OF V/STOL MODELS

By Harry H. Heyson  
NASA Langley Research Center

### SUMMARY

Considerable care is required in applying wall interference corrections to V/STOL data. The following items comprise a minimum list of features which should be considered: type of tunnel and proportions, effective wake skew angle, span of both lifting system and tail, configuration, model location, tail length and height, angle of attack, pivot location, and center-of-gravity location. Auxilliary balances may be required to obtain the forces of each component in complex lifting systems. Some discrepancies may remain, largely because of the imperfect knowledge of the aerodynamics of many V/STOL configurations. The boundary layer on the tunnel floor requires careful consideration, particularly in ground-effect testing. Recirculation will limit the minimum speeds at which successful data can be obtained. Many questions, such as the effect of angular and velocity rates, remain to be answered in evaluating V/STOL testing techniques.

### INTRODUCTION

Present V/STOL test technique in wind tunnels differs only slightly from the techniques used for years in powered model testing. Considerable skill and ingenuity may be required in order to actually package the large power requirements in a model of suitable size. Even more ingenuity may be required to carry the required power, whether it be electric, pneumatic, or hydraulic, across the balance without engendering exorbitantly large or unrepeatable tares. However, once these problems are overcome, the test program settles down to producing systematic sets of data for incremental changes in the almost innumerable adjustments built into the model.

One practical difficulty is that the usual V/STOL model does have so many possible configuration changes and adjustments. The test program becomes so long that it becomes very tempting to economize on occupancy time and cost by omitting the tedious and time-consuming runs to obtain such items as strut tares. This omission is not always justified, particularly when unshielded portions of the struts, and their junction with the model may be bathed in a propeller slipstream or a jet exhaust.

An additional problem is that small Reynolds number may present difficulties in evaluating the test data. Reasonable rules have been worked out to extrapolate drag results to higher Reynolds number. Unfortunately, in V/STOL testing, the scale effects of interest are usually those involving separations; that is, maximum lift, maximum turning angle, etc. The effect of Reynolds number on these phenomena is not consistently predictable and can lead to many

surprises - both pleasant and unpleasant.

On the other hand, there really are some significant differences between conventional and V/STOL testing. The present lecture will address itself to several of these differences. Primary attention will be given to wall interference which, under certain circumstances, may be an order of magnitude larger than in conventional testing (ref. 1). Requirements for ground-effect tests are discussed. The recent developments in determining the minimum speed at which V/STOL tests can be run in a wind tunnel are presented. Finally, some questions are raised about the adequacy of steady state wind-tunnel testing in the determination of V/STOL transition characteristics.

### SYMBOLS

A	aspect ratio
$A_M$	momentum area of lifting system
$A_T$	cross-sectional area of test section
b	distance from center of model (or wake) to right-hand side wall (as viewed from behind)
b	wing span
B	semiwidth of wind tunnel
$C_L$	lift coefficient, $L/qS$
D	diameter of jet
h	height of model above ground plane or tunnel floor
H	semiheight of wind tunnel
L	lift
$L_N$	relative-lift factor of element of lifting system
$m^*$	doublet strength
$M_T$	mass flow through wind tunnel, $\rho A_T V$
$M_u$	mass flow of model from drag, defined as $\rho A_M u_0$
$M_w$	mass flow of model from lift, defined as $\rho A_M w_0$
M,N	integers

$q$	dynamic pressure
$q_c$	corrected dynamic pressure
$R$	rotor radius
$s$	wing semispan
$S$	wing area
$t$	time
$u_0$	mean, or momentum theory, value of longitudinal induced velocity at lifting system, positive rearward
$\Delta u$	total longitudinal interference velocity
$\Delta u_D$	longitudinal interference velocity due to drag
$\Delta u_L$	longitudinal interference velocity due to lift
$V$	free-stream, or tunnel, velocity
$V_j$	jet exit-velocity
$w_0$	mean, or momentum theory, value of vertical induced velocity at lifting system, positive upward
$\Delta w$	total vertical interference velocity
$\Delta w_D$	vertical interference velocity due to drag
$\Delta w_L$	vertical interference velocity due to lift
$x, y, z$	distances from origin to a given point, measured along tunnel axes, x positive rearward, z positive upward, y to form a right-hand system
$\alpha$	angle of attack
$\Delta\alpha$	correction to angle of attack
$\gamma$	ratio of tunnel semiwidth to semiheight, $B/H$
$\Gamma$	circulation
$\delta$	interference factor, either classical or in general
$\delta_{u,D}$	interference factor defining longitudinal interference due to drag

$\delta_{u,L}$	interference factor defining longitudinal interference due to lift
$\delta_{w,D}$	interference factor defining vertical interference due to drag
$\delta_{w,L}$	interference factor defining vertical interference due to lift
$\epsilon$	mean downwash angle at lifting system, positive downward from tunnel axis
$\epsilon_e$	effective mean downwash angle
$\zeta$	height parameter, $H/h$
$\eta$	lateral position parameter, $b/B$
$\theta$	angular position of model in pitch
$\theta_j$	initial inclination of jet axis, positive rearward from vertical
$\Lambda$	wing sweep angle
$\rho$	mass density of air
$\sigma$	ratio of model span to tunnel width, $\frac{2s}{2B}$ or $\frac{2R}{2B}$
$\sigma_T$	ratio of tail span to tunnel width
$\chi$	wake skew angle, measured positive rearward from negative vertical wind tunnel axis
$\chi_e$	effective wake skew angle
Subscripts	
$( )_N$	pertaining to Nth wake
$( )_{N,M}$	effect of Nth wake at Mth point

## WALL EFFECTS

### CLASSICAL CORRECTIONS

Prandtl, Glauert, Theodorsen (refs. 2 to 4) and a host of successors developed the classical wind-tunnel corrections. These theories lead to a change in effective angle of attack in the tunnel given by

$$\Delta\alpha = \delta \frac{S}{A_T} C_L \quad (1)$$

where  $\delta$  is a constant which depends upon a number of wind-tunnel and model configuration parameters. The initial problem in applying these theories to V/STOL testing was that the correction angle  $\Delta\alpha$  appeared to approach infinity as  $C_L$  grew without bound when the velocity decreased toward zero. Actually this result was not correct since the actual equation, without small angle assumptions, was

$$\tan \Delta\alpha = \frac{\Delta w}{V} = \delta \frac{S}{A_T} C_L \quad (2)$$

Thus,  $\Delta\alpha$  approached  $90^\circ$  rather than infinity as  $C_L$  approached infinity. This result merely indicates that an upwash is present even when the velocity is zero.

### NASA Technical Report R-124

As indicated in figure 1, the classical theory assumed that the wake passed directly downstream without deflection from the horizontal. This assumption is severely violated in V/STOL testing, where the wake is deflected violently downward in order to obtain lift at very small forward speed. A newer theory, built upon earlier work for the helicopter, was presented in NASA TR R-124 (ref. 5). In this analysis, the wake was assumed to be deflected downward, following a straight-line path, until it met the floor, after which it ran off along the floor.

No real wake behaves in such a simple straight-line fashion; however, numerous experimental studies, as well as some theoretical work to be discussed subsequently indicate that this simple representation does indeed seem to yield reasonable results.

The interference of the walls is expressed somewhat differently in the theory of reference 5. Four interferences are found as

$$\begin{aligned}\Delta w_L &= \delta_{w,L} \frac{A_M}{A_T} w_0 \\ \Delta u_L &= \delta_{u,L} \frac{A_M}{A_T} w_0 \\ \Delta w_D &= \delta_{w,D} \frac{A_M}{A_T} u_0 \\ \Delta u_D &= \delta_{u,D} \frac{A_M}{A_T} u_0\end{aligned}\quad (3)$$

Note that the "lift interference" has two components, vertical and horizontal, as does the "wake-blockage interference." These are expressed as functions of the mean induced velocities at the lifting system rather than in terms of  $C_L$ . Note also, that the momentum area, rather than the wing area, is used in the definition. For a wing, this is the area of the circle circumscribing the wing tips. As a result of the differences in definition, there will be a constant factor of -4 between the  $\delta$  of classical theory and  $\delta_{w,L}$  of reference 5.

In applying equations (3), it will be noted that the total interferences are

$$\begin{aligned}\Delta w &= \Delta w_L + \Delta w_D \\ \Delta u &= \Delta u_L + \Delta u_D\end{aligned}\quad (4)$$

after which

$$\begin{aligned}\Delta \alpha &= \frac{\frac{\Delta w}{V}}{1 + \frac{\Delta u}{V}} \\ \frac{q_c}{q} &= \left(1 + \frac{\Delta u}{V}\right)^2 + \left(\frac{\Delta w}{V}\right)^2\end{aligned}\quad (5)$$

Several interesting points may be noted about this correction system. A sample set of interference factors is presented in figure 2. The factors, as a function of the wake skew angle  $\chi$ , are for a vanishingly small model centered in a closed wind tunnel having a width-height ratio of 1.5. Note that at  $\chi = 90^\circ$ , which corresponds to the classical undeflected wake, three of the four factors are zero, and only  $\delta_{w,L}$  has a value. Other than the factor of -4 due to the different definition,  $\delta_{w,L}$  at  $\chi = 90^\circ$  corresponds exactly to the classical  $\delta$ . Thus the newer theory yields precisely the same result as classical theory when the wake is undeflected. Note however, that large wake deflection can substantially alter the wind-tunnel interference from the classical case.

A second interesting point may be made if equations (3) are divided by  $V$  and then multiplied on the right-hand side by  $\rho/\rho$ , to yield

$$\begin{aligned}\Delta w_L &= \delta_{w,L} \frac{\rho A_M w_0}{\rho A_T V} = \delta_{w,L} \frac{M_w}{M_T} \\ \Delta u_L &= \delta_{u,L} \frac{\rho A_M w_0}{\rho A_T V} = \delta_{w,L} \frac{M_w}{M_T} \\ \Delta w_D &= \delta_{w,D} \frac{\rho A_M u_0}{\rho A_T V} = \delta_{w,D} \frac{M_u}{M_T} \\ \Delta u_D &= \delta_{w,D} \frac{\rho A_M u_0}{\rho A_T V} = \delta_{u,D} \frac{M_u}{M_T}\end{aligned}\quad (6)$$

Since  $\rho A_M V$  is the mass flow through the wind tunnel and  $\rho A_M w_0$  and  $\rho A_M u_0$  are, in a sense, mass flows due to the lifting system's own induced velocities only. Thus the wind-tunnel interference is a function of the ratio of the model mass flows to the wind-tunnel mass flow. Note that  $M_u$  and  $M_w$  are not really the actual mass flows which actually depend upon the resultant velocity and thus also include some effects of forward velocity as well.

#### EXPERIMENTAL INVESTIGATIONS

A wide variety of experimental investigations (refs. 6 to 11) have been conducted by several organizations and on many widely differing configurations (figs. 3 to 5) in order to obtain verification of the theory of reference 5. In general, substantially improved agreement was obtained between sets of data obtained in different wind tunnels. On the other hand, as is often the case, the experiments pointed up several factors which required careful attention and even reevaluation. As anticipated by TR R-124, it was shown necessary to account for both the finite size and geometric arrangement of the model configuration in calculating the interference factors. This point will be discussed

subsequently in some detail. Of more immediate concern, however, was the anomalous corrections obtained for pitching moments for some configurations, such as the fan-in-wing model. In this particular case, correction actually increased the differences between wind tunnels.

#### EFFECTIVE WAKE SKEW ANGLE

Intensive study of the problems of pitching moment due to the tail finally pinpointed the problem as the wake skew angle. In the absence of adequate experimental studies at the time, reference 5 had assumed that this wake skew angle could be taken as the angle defined at the lifting system by momentum theory (ref. 12). The final result is that this assumption was not really true. The wake rolls up almost immediately for the lift coefficients and aspect ratios of interest to  $V/STOL$  aircraft, and, under these circumstances, the wake skew angle is substantially altered.

The effect of roll-up on the skew angle (or its complement, the deflection angle) may be seen most clearly in the case of a wing. Figure 6 shows a wing with the simple horseshoe vortex system that it has under fully rolled-up conditions. At the center of the wing, the bound vortex has no effect and each of the trailing vortices yields an induced velocity of  $w_0/2$ . Thus the total induced velocity at the lifting system is  $w_0$ . In the far wake, the bound vortex again has no effect because of its great distance. Each trailing vortex, being essentially doubly infinite in length, contributes an induced velocity  $w_0$  at the center of the wake so that the induced velocity at the center is  $2w_0$ . This is, of course, the same result as the simple momentum theory. On either trailing vortex, however, the only effective vortex is the opposite vortex. This second vortex being twice as far away from the first vortex as it is from the center contributes an induced velocity of only  $w_0/2$ . Thus, the final result is that the mass flow of the system, being confined between the trailing vortices, does double its downward velocity in the far wake; however, the trailing vortices themselves proceed downward in the far wake with only half the induced velocity that they had at the center of lift.

The same result holds true for more complex lifting systems. Figure 7 shows contours of vorticity (from ref. 13) measured immediately behind a helicopter rotor. Since the wake, in this case, is pictured as a skewed cylindrical sheet of vorticity, it would be expected that the vorticity would be found at, or within, the intersection of this cylinder and the plane of the survey. (This intersection is the dashed ellipse shown in the lower portion of the figure.) The experimental contours, however, leave no doubt that the wake is essentially completely rolled up into a trailing vortex pair. Furthermore, these rolled-up vortices have progressed downward only half as far as would be expected if they traveled downward with the velocity calculated at the center of the disk.

It should be noted that it is only the far field of the lifting system which is of interest in wall-interference calculations. Furthermore, it is only the wake vorticity, and its position, that determines the interference factors. Thus it appears (ref. 10) that the wake skew angle of reference 5

should be interpreted (as in the remainder of this lecture) as being some effective wake skew angle differing from the momentum skew angle. In particular, to a first approximation if  $\epsilon$  is the downwash angle at the center of the lifting system

$$\epsilon_e = \epsilon/2 \quad (7)$$

and since  $\chi$  is the complement of  $\epsilon$

$$\chi_e = \frac{\chi + 90^\circ}{2} \quad (8)$$

Equations (7) and (8) are obviously not correct in pure hovering where the wake vorticity does indeed pass downward at  $\chi = 0^\circ$ . Thus, some reasonable small forward (or wind-tunnel) velocity is assumed. Actually, recirculation effects, which will be discussed in a subsequent section, limit the minimum speed at which valid wind-tunnel data can be obtained. Thus, equations (7) and (8) will probably be sufficient for practical use.

#### CONSIDERATIONS IN CALCULATING WALL INTERFERENCE

NASA TR R-124 primarily presents only interference velocities along the wind-tunnel axes for a vanishingly small model. Sample calculations, made for a few multiple-element and finite-size systems are also given and indicate significant effects. Because of the wide variety of configurations employed in V/STOL work, as well as because of the fact that the corrections also depend upon wake deflection, the preparation of tables of interference factors for all possible sizes and types of configurations is totally uneconomic. Thus, the published tables (refs. 14 to 18) are limited to the vanishingly small model case. The individual user must then consider the effects on his own configuration and utilize superposition techniques and supplemental calculations to obtain the appropriate factors for his own model. To this extent, reference 5 presents a "thinking-man's" set of corrections. The following sections discuss several features which should be considered.

Interference at tail. - The first item to be discussed is the interference at the tail. This interference is, of course, not generally identical to that at the lifting system. Thus, there will be a correction, primarily to pitching moment, that will depend basically upon the differences in interference between the tail and the center of lift (refs. 19 and 20). Note, however, that the position of the tail in the wind tunnel will change as a function of the model angle of attack. Thus, if the effective pivot point is at the center of lift, the tail will be low in the tunnel at positive angle of attack and high at negative angle of attack.

Figure 8 displays the correction factors ( $\delta_{w,L}$ ) for a tail mounted one tunnel semiheight behind a vanishingly small model centered in a closed wind tunnel having a width-height ratio of 1.5. The corresponding values for the center of lift and for the tail with angles of attack of  $\pm 10^\circ$  are also shown. (In this, and succeeding figures, only  $\delta_{w,L}$  is shown for reasons of brevity. In most cases,  $\delta_{w,L}$  accounts for the bulk of the wall interference. It should be noted, however, that the effects illustrated will also be evidenced to some degree in the other three interference factors as well.)

It may be seen that the effect of angle of attack is small and symmetrical about  $\alpha = 0$  when the wake is horizontal ( $\chi = 90^\circ$ ). When the wake is deflected substantially, the effect of angle of attack becomes quite large. Indeed, at low skew angles (say  $\chi = 45^\circ$  to  $50^\circ$ ) the effect of changing the angle of attack from  $0^\circ$  to  $10^\circ$  is almost as large as the difference between the center of lift and the tail at  $\alpha = 0$ . It is evident that this effect is large enough so that its consideration should be included in any correction scheme. Note that a change in tail height of the model will have similar effects.

Superposition techniques for finite size models. - As pointed out in reference 5, superposition techniques may be used to obtain the appropriate factors from that paper for finite size models. At the outset, it is valuable to examine the wake assumed in reference 5 so as to see the reasons for the selection of this particular wake model.

The upper left-hand corner of figure 9 shows the wake of a helicopter rotor as often visualized in theoretical rotor wake studies (for example, ref. 13). It is a skewed cylindrical vortex cylinder composed of a uniform distribution of vortex rings such as the one shown darkened. Now it is possible to substitute a uniform distribution of doublets over the area circumscribed by the ring for the ring itself as indicated in the second sketch. Finally, if the distance from the wake is reasonably large, the solid angle subtended by each ring becomes quite small. Thus a point doublet can be substituted for each of the disk-shaped distributions of doublets. The final wake is thus a line of such doublets lying skewed across the main flow.

The same wake is obtained by considering a wing as indicated in the lower portion of figure 9. Here the horseshoe vortex is replaced by a rectilinear sheet of uniformly distributed source-sink doublets. At sufficient distance from the wake, the angle subtended across the wake becomes so small that the wake may be considered as a line of point doublets.

Note that in the limit of a small model, there is no real difference between the wake of a wing and of a rotor. There are differences in the angles of inclination of the doublets; however, reference 5 treats this effect by working first with a case in which the axes are vertical and then with a case in which the axes are horizontal. The correct inclination is then obtained by superimposing the two cases with strengths according to the model lift and drag. One other point is noteworthy in that classical theory has often used a vortex doublet rather than source-sink doublets. The present representation is superior in that it includes the effect of the bound vortex.

Since the representation used in reference 5 seems to cover such a wide variety of possible models, it is evident that individual finite model configurations can be "built-up" by a suitable distribution and summation of the effects of a large number of so-called vanishingly-small wakes. Some sample calculations were included in the original paper; however, the procedure may be greatly simplified for a number of standardized configurations. One example will be presented in the following section.

Interference factors for swept wings of finite span. - Consider a swept wing located in the wind tunnel as indicated in figure 10. The apex of the swept lifting line is chosen as the origin and point of reference. The location of the wing in the tunnel is given by  $\zeta$  (the semiheight of the tunnel divided by the height of the model apex) and  $\eta$  (the distance from the apex to the right-hand wall divided by the semiwidth). The model span is defined by  $\sigma$  (ratio of semispan to tunnel semiwidth). The span is then divided into 10 equal parts, numbered  $N = 1$  to 10 starting from the right-hand tip, and each segment is represented by a vanishingly small wake originating at its midpoint. For a given sweep angle  $\Lambda$  and angle of attack  $\alpha$ , the coordinates of the origin of each wakes are

$$\begin{aligned} \left(\frac{x}{H}\right)_N &= \left| \frac{11 - 2N}{10} \right| \sigma \gamma \tan \Lambda \cos \alpha \\ \left(\frac{y}{H}\right)_N &= \frac{11 - 2N}{10} \sigma \gamma \\ \left(\frac{z}{H}\right)_N &= - \left| \frac{11 - 2N}{10} \right| \sigma \gamma \tan \Lambda \sin \alpha \end{aligned} \tag{9}$$

In order to obtain the contribution of any individual wake to the interference at any given point, it is necessary to find the individual  $\zeta$  and  $\eta$  of that wake and to find the coordinates  $\left(\frac{x}{H}\right)$ ,  $\left(\frac{y}{H}\right)$ ,  $\left(\frac{z}{H}\right)$  of the point in question as measured from the individual wake. To find the total interference at a point, it is necessary to sum the contributions of all ten wakes at that point and then to readjust the values to unit lift (that is, the sum of the strengths of the wakes must equal the unit strength assumed in the theory). Finally, to obtain the average interference, the total interference at  $M$  points across the span must be averaged. If  $M$  is chosen to represent 10 points coincident with the origins of the original 10 elementary wakes, the result may be written as

$$\delta = \frac{1}{10} \sum_{N=1}^{10} \sum_{M=1}^{10} L_N \cdot \delta \text{ at } \left\{ \begin{array}{l} \zeta_N = \frac{\zeta}{1 - \left| \frac{2N - 11}{10} \right| \sigma \gamma \zeta \tan \Lambda \sin \alpha} \\ \eta_N = \eta + \frac{2N - 11}{10} \sigma \\ \left( \frac{x}{H} \right)_{N,M} = \sigma \gamma \tan \Lambda \cos \alpha \left[ \left| \frac{11 - 2M}{10} \right| - \left| \frac{11 - 2N}{10} \right| \right] \\ \left( \frac{y}{H} \right)_{N,M} = \frac{\sigma \gamma}{5} (N - M) \\ \left( \frac{z}{H} \right)_{N,M} = \sigma \gamma \tan \Lambda \sin \alpha \left[ \left| \frac{11 - 2N}{10} \right| - \left| \frac{11 - 2M}{10} \right| \right] \end{array} \right\} \quad (10)$$

where each individual wake has been assigned an arbitrary strength of  $L_N$ . The form of the equation is independent of which interference factor is being calculated, just so that  $\delta$ 's under the summation signs are identical to the type of final  $\delta$  being sought.

The actual values required for the evaluation of equation (10) can be obtained by interpolation from published tables (refs. 14 to 18). Since 100 values are actually required in this case, such hand labor is quite tedious. It is more profitable to program equation (10) along with the equations of reference 5 and then do all of the manipulation within an electronic computer. In the CDC 6600 computer at the Langley Research Center, the correction factors for eight skew angles are obtained in 12 minutes (or 6 minutes for symmetric cases with  $\eta = 1$ ).

Note that, with suitable changes in notation, equation (10) is valid for any linearized correction theory which will give the interference for a vanishingly small element, arbitrarily located in the tunnel, at an arbitrary point in the tunnel.

The interference distribution is obtained simply by dropping the normalizing constant of  $1/10$ , omitting the summation on  $M$ , and computing equation (10) individually for all  $M$ 's. Only minimal alterations are required to obtain the average interference over a finite-span tail behind the finite span wing.

Several similar programs are already operational at the Langley Research Center. These include the swept wing, rotors or propellers, and an arbitrary array of lifting jets. In each case, the average interference, the interference distribution, and the average interference at the tail are considered. In each case, there is also some choice of load distribution built into the programs. Wings may have uniform or elliptic loading; rotors may have uniform or triangular loading; and the jet programs allow completely arbitrary choice of loading.

Effect of finite span - straight wings. - Values of  $\delta_{w,L}$  have been calculated for a series of finite span straight wings mounted in the center of a closed tunnel having width-height ratio of 1.5. These values are presented in figure 11. Significant effects are evident. It is thus necessary to account for the finite size of the model on the average corrections.

The interference distribution across the wing is also of interest and is shown, for  $\chi = 60^\circ$ , in figure 12. Very significant differences in the distribution over the span are evident. For the smaller wings, there is a small decrease in interference toward the tips; for the largest wing ( $\sigma = .75$ ), there is a substantial increase in upwash toward the tips. Actually correcting data for such alterations in interference distribution is difficult and is seldom attempted in practice. Nevertheless, substantial effects may be observed, particularly with respect to the measured stall angle. This angle may be either increased or decreased depending, not only on the span-width ratio, but also upon whether the wing has an initial tendency to stall at the wing root or at the wing tip.

Effect of sweep and angle of attack. - Under the lifting-line assumptions used in deriving the interference for finite span wings, there is no effect of angle of attack on the interference factors for a straight wing. It will also be noted that the inclusion of sweep requires a consideration of the effect of angle of attack as well since, as the angle of attack varies, the relative positions of the various elements of the wing also vary.

Figure 13 compares the interference factors for a swept wing ( $\Lambda = 45^\circ$ ) at angles of attack of  $0^\circ$  and  $20^\circ$  with the corresponding factors for a straight wing. In all cases, the aerodynamic center of the wing is in the center of the closed tunnel. It is evident that the effects of sweep and angle of attack are comparatively small in this case. (This result is peculiar to the centered location of the model; significant differences may be obtained if the model is located substantially above or below the centerline.) Despite the close similarity of the average interference factors, large differences occur in the distribution of interference over the model (fig. 14). As noted earlier, the distribution across the straight wing is such that the interference decreases somewhat toward the tips. In contrast, for the swept wing, the interference at the tip is essentially twice as great as the interference at the root in the case shown. The effect of angle of attack is comparatively smaller. The large gradients illustrated in figure 14 would be expected to aggravate the usual tendency of highly swept wings to experience an early tip stall.

Effect of pivot point on interference for swept wings. - Since the derivation for the interference used the apex of the lifting line as the origin, an alteration in the height parameter was required in order to obtain interference

factors for a case in which the aerodynamic center was fixed at the tunnel center. That is, the necessary alterations were made to insure that the wing pivoted about the aerodynamic center as the angle of attack was changed.

Figure 15 compares the interference factors calculated with the pivot at the aerodynamic center with those calculated when the pivot is at the apex of the lifting line. The effect of the choice of pivot location is shown to be larger than the effect of either sweep or angle of attack by themselves. The result is not unanticipated for, at  $\alpha = 20^\circ$ , the average location of the wing in the tunnel is substantially lower when the pivot is at the apex than it is when the pivot is at the aerodynamic center.

It is obvious that the effective pivot point locations should be considered when correcting data. It might be well to consider this point in planning the tests as well, since a favorable choice can reduce the changes in correction factor with angle of attack. Features such as pivot point location make it very difficult to correct someone else's data after publication since items such as pivot location are seldom given in the final report.

Effect of sweep on interference at tail. - In contrast to the very small effect of sweep at the lifting system, sensibly large effects are obtained at typical tail locations. Figure 16 shows the calculated interference over a zero-span tail behind straight and swept wings at two angles of attack. The differences shown are significant. The omission of sweep in a case such as this could result in a 10-percent error in interference at the tail.

Effect of tail span on interference at the tail. - Most calculations of interference at the tail omit any effect of tail span. This omission follows precedents developed during the 1930's and 1940's when the tail span was usually small compared to the wing span. Many V/STOL configurations have abnormally large tails in an attempt to retain some tail effectiveness at very low transition speeds. Figure 17 displays the calculated interference factors for tail spans of zero and of half the wing span behind the same swept wing as the previous figure. The effect of tail span in this example is greater than the effect of  $45^\circ$  of sweep. At  $\alpha = 20^\circ$ , the combined omission of wing sweep and tail span may result in errors of as much as 25 percent of the interference at the tail.

Interference for rotors. - The average interference for a lifting rotor of finite span is calculated in a manner analogous to that previously shown for the swept wing. The values to be shown herein were computed from a wake configuration consisting of 20 individual "vanishingly-small" wakes.

Figure 18 shows the average interference for a rotor whose diameter, or span, is equal to half the wind-tunnel width. These interference factors are compared with the corresponding factors for a wing of the same span, as well as those for a vanishingly small model. Again significant differences are seen, not only as a result of span, but also as a result of the differences in configuration when the span is finite. The interference factors are slightly larger for the rotor than for the wing as might be expected because of the large longitudinal extent of the rotor and the downstream growth of interference in the tunnel.

Effect of  $\alpha$  on interference for rotors. - Figure 19 shows the effect of changes in angle of attack for the same lifting rotor. In this case, significant differences are observed at the lower skew angles. Other things being equal, a rotor at positive angle of attack will experience a somewhat greater wall interference than a rotor at negative angle of attack. Even in this case, angle of attack can result in fairly significant differences in interference distribution. Figure 20 shows the distribution over the longitudinal axis of the rotor at a skew angle of  $60^\circ$ . At this skew angle, the average interference factors for the three angles of attack are virtually identical; however, the distributions on the longitudinal are significantly different. The largest differences occur near the tips of the rotor where the interference will be most effective (because of the long lever arm) in producing changes in either the rotor pitching moment or flapping (refs. 21 and 22).

The notation used in these wind-tunnel interference studies can be quite confusing when applied to rotors. Skew angle, which in rotor downwash studies, is referenced to the normal to the tip-path plane, is referenced to the vertical wind-tunnel axis herein. Angle of attack has a multiplicity of definitions in rotor theory. The  $\alpha$  desired in applying wind-tunnel interference calculations is the angle of attack of the tip-path plane.

Complex models. - Thus far the discussion has centered on comparatively simple models such as wings and rotors. Unfortunately, most V/STOL models are far from simple; thus, a few comments on the interference for more complex systems are in order.

Figure 21 illustrates by sketches a few of the systems used on V/STOL aircraft. In the case of configurations, typified by the deflected-slipstream, tilt-wing, and jet-flap systems, the entire wake more or less blends together at the lifting system and leaves as a conglomerated unit provided that some reasonable forward velocity is present. In such cases, it appears best to consider the entire system as a roughly equivalent wing. Experimental results indicate this procedure is reasonably adequate.

A second class of possible models is typified by lift-jet and fan-in-wing configurations. In these systems, the lifting elements are closely coupled; however, because of the large difference in wake velocity, the wakes maintain their separate identities. In these cases, it is necessary to compute the interference of the various lifting elements upon themselves and the other components and to sum these interferences appropriately. The application of corrections in this manner requires that the forces produced by each segment of the lifting system be known. It is not adequate to know only the total forces generated by the entire configuration. Furthermore, these forces cannot be determined from simple "build-up" tests since the direct interference between elements is large. Thus, it is necessary to install internal auxiliary balances to measure independently the forces generated by each element. In the absence of such auxiliary balances, it may not be possible to correct the data with a satisfactory degree of accuracy.

Multi-element systems. - The lift-jet and fan-in-wing systems described above are closely coupled examples of a more general class of multi-element lifting systems. If the coupling is not as close, it may be possible to examine

the interference and distribution of interference over each element, and in some cases, to compute and correct for the interference on each element of the system. A few examples are shown in figure 22.

First consider a tandem rotor helicopter. Each rotor experiences a wall interference due to its own presence in the wind tunnel. Each also experiences a wall interference due to the presence of the other rotor in the wind tunnel. The correction at each rotor is the sum of the interference due to its own presence and the interference due to the presence of the rotor. The total interference at each rotor is thus a function of the operating conditions of both rotors. These must be known independently of each other while operating in the presence of each other.

The problem is further complicated by the fact that the rotors change their positions relative to each other and to the walls as the angle of attack is varied. Furthermore, the angles of attack of the front rotor, rear rotor, and the fuselage will, in general, all be different and, for flapping rotors, will vary as a function of the operating condition. A complete examination of the interference for such a system is behind the scope of this paper; however, a few numerical results for a simplified case will be given in the next section.

The unloaded rotor is another interesting case. Here the wing and rotor experience individual interferences which are the sum of the effect of their own presence and the effect of the presence of the opposite element. The angles of attack and skew angles of each element are greatly different and the positions of the elements with respect to each other again vary, but to a smaller degree. The tail, of course, sees an interference which is the sum of the effects due to the presence of both the wing and the rotor.

The tilt rotor is a somewhat more complicated variant of the unloaded rotor. In this case, three elements are present and the interference at any one element is the sum of the interference incurred by the presence of all three elements (as is the interference at the tail). The situation is relieved to a small extent by the fact that the two rotors must be trimmed to produce identical resultant forces in order to avoid large rolling or yawing moments. On the other hand, large effects of angle of attack of the rotors must be expected since the rotors change angle of attack by  $90^\circ$  as the conversion maneuver progresses from hovering to high-speed forward flight. Note also that the corrections will vary not only as a function of fuselage angle of attack, but also as a function of the mast (or tilt) angle of the rotors. The latter effect will occur because of the large alterations in relative positions of wing and rotors as the transition progresses

Sample results for tandem rotors. - A few calculations of the longitudinal interference distribution are presented for tandem rotors. The system is assumed to pivot in angle of attack about the hub of the front rotor. The rotors are assumed to lie in the same plane with zero overlap. This assumption amounts to restricting the angles of attack of the two rotors and the fuselage to be identical. The wake skew angles of both rotors are assumed to be  $60^\circ$  irrespective of changes in angle of attack, comparative operating conditions, and mutual interference. The correction factors to be presented will be based always on the momentum area of one rotor and on the average  $w_0$  for the rotors. Although the

foregoing assumptions are somewhat restrictive, the general magnitude of the calculated effects should be indicative of the trends to be expected.

The interference factors presented in figure 23 show the interference caused by the presence of each rotor over the entire length of the tandem system at  $\alpha = 0$ . The contributions of the two rotors are identical in this case except for a change in longitudinal position which is referenced to the center of the front rotor in figure 23. The rear rotor contribution at the front rotor is small, but does slightly increase the gradient of interference over the front rotor. The front rotor contribution over the rear rotor is large and produces major changes in both the average value and the slope of the interference at the rear rotor. The total interference is the sum of the two interferences and is shown by the solid line in figure 23. The magnitude of the interference velocity is quite large. It will be noted that, for either rotor of the tandem pair

$$\frac{A_M}{A_T} = \frac{\pi (\sigma B)^2}{4 B H} \quad (11)$$

but

$$H = \frac{H}{B} B = \gamma B$$

so that

$$\frac{A_M}{A_T} = \frac{\pi \gamma \sigma^2}{4} \quad (12)$$

Then, from the definition of  $\delta_{w,L}$

$$\frac{\Delta w_L}{w_0} = \delta_{w,L} \frac{\pi \gamma \sigma^2}{4} \quad (13)$$

or, in the present case ( $\gamma = 1.5$ ,  $\sigma = 0.5$ )

$$\frac{\Delta w_L}{w_0} = 0.295 \delta_{w,L} \quad (14)$$

From figure 23, it may be seen that the average value of the total interference over the rear rotor is on the order of -1.8. Thus, the average interference velocity at the rear rotor is about equal to one-half of that rotors own mean induced velocity. On the other hand, the total interference velocity at the front rotor is only on the order of 15 percent of its mean induced velocity. Interferences, and differences in interference of these magnitudes, will produce impossibly large changes in relative loading and pitching moment of the system. The implications of figure 23 are that the total length of a tandem rotor model should be no greater, and preferably less, than the diameter of an acceptably sized single-rotor model.

Figure 24 shows the effect of angle of attack on the distribution of total interference for the same tandem system. In this case, extreme differences are noted. This result might be expected from the previous consideration of the tail behind a lifting model since the rear rotor translates vertically over large distances as the angle of attack is changed. Note that the total load interference over the rear rotor may be well in excess of three times the rotors own induced velocity when the angle of attack is positive.

Reduction of model size is multiply beneficial in a case such as this. The interference is reduced directly as a function of area; the length is reduced so that the motion of the rear rotor with angle of attack (and consequently the effect of  $\alpha$  on interference) is reduced; and drawing the rear rotor closer to the front rotor (in terms of tunnel dimensions) reduces the degree by which the front rotor interference factors grow over the distance occupied by the rear rotor.

For stability reasons, as well as to slightly off-load the rear rotor which must operate in the downwash of the front rotor, the center of gravity of a tandem rotor system is usually located forward of the midpoint between the two rotors. The foregoing results were calculated assuming the center of gravity to be at the midpoint. In actual practice, the effect of center-of-gravity location will appear in the  $w_0$  term when evaluating the poritions of total interference contributed by each rotor; however in the present case, where the interference factors are based on the average  $w_0$ , the equivalent result can be obtained by suitably biasing the interference factors contributed by each rotor before adding to obtain the total interference.

Figure 25 compares the interference distributions, obtained in this manner, for centers of gravity located at the midpoint and for a center of gravity which is 10-percent (of the distance between rotors) forward of the midpoint. The differences are sufficiently great to indicate a need to consider the center-of-gravity-location in applying corrections.

Treatments of nonuniform interference. - Thus far, it has essentially been assumed that, if the actual distribution of a nonuniform interference field is known, it is possible to compute the effect of the nonuniform field and then remove this effect from the data. For some simple configurations such as isolated rotors, propellers, or wings, this procedure is reasonable since the underlying theory exists.

A simple case, in example, is the rotor. The effect of a linear gradient of interference (or induced) velocity has been shown to produce an alteration in only the lateral flapping if the rotor is fitted with flapping hinges at its center (ref. 21). If the rotor is completely rigid, the equivalent effect is a large pitching moment (ref. 22). On the other hand, if the rotor is fitted within a wing, such as in the fan-in-wing configuration, no theory presently exists which is capable of evaluating the effect of the same gradient.

Except for a few cases, such as those mentioned earlier, no general theory exists by which the effect of arbitrary nonuniform interference fields upon an arbitrary model can be calculated. Thus the complete correction of V/STOL wind-tunnel data, may not always be possible, particularly with respect to moments. Such effects are not really chargeable as errors in wall-effects theory, which merely provides the interference velocity field. Instead, the errors in correction caused by such effects are chargeable to the abysmally inadequate state of theoretical knowledge of the aerodynamics of many V/STOL configurations.

Even though complete correction may not always be possible, there are certain physical equivalence concepts (ref. 23) which can be used to obtain an indication of the magnitude and direction of the effect of nonuniform interference. For example, as in figure 26, the nonuniform interferences can be considered as an effective aerodynamic warping or distortion of the model into a slightly different configuration.

The effect of a nonuniform lateral gradient of vertical interference on a wing, for example, produces the same lateral distribution of section angle of attack that would be obtained on a model with an altered twist distribution. Thus, the model may be considered as equivalent to a wing of different twist in free air. Similarly, as indicated in figure 26, a longitudinal gradient of vertical interference produces a curved flow. An airfoil operating in this curved flow is equivalent to an airfoil with slightly different camber in free air. When the effects of this curved flow on a complete model are considered, it will be noted that the equivalent model in free air also has an altered tail setting and tail height.

Nonuniform interference can also be considered as equivalent altered operating condition in free air. To the extent that a gradient is uniform, as in figure 27, the effect of the nonuniform field is the same as though the model was operating in free air at an angle of attack altered by a  $\Delta\alpha$  defined by the average interference and a rate of rotation

$$\frac{d\theta}{dt} = \frac{d(\Delta w)}{dx} \quad (15)$$

Note also that instead of altering  $\alpha$ , the model in free air could have been considered to be operating at the unaltered angle of attack but at a rate of descent equal to  $\Delta w$ . This latter concept can be particularly helpful since the effects of rotation rates are of importance in stability work, and theoretical and empirical formulas can often be found in the published literature.

Wake curvature. - The theory of NASA TR R-124, as noted earlier, assumes that the wake passes downward and rearward in a straight line until it intersects the floor. In actual fact, however, the wake does not travel in a straight line but follows a curved path. The use of an effective wake skew angle largely, but not totally, corrects for this curvature. The extent of the possible differences will be discussed in this section.

The most notable deviations from a straight-line wake occur with lift-jet wakes. The shape of such a wake is visualized by injecting water into the flow through a simple nozzle is shown in figure 28. The curvature of the wake is seen to be large. Flow studies indicate that the curvature is associated, at least in part, with a roll-up process in which the initial circular wake shape is transformed into a closely coupled vortex-pair. The theoretical calculation of such paths is fraught with difficulty, and has not yet been completed; however, Margason, at the Langley Research Center, has developed the following equation which seems to predict, with reasonable accuracy, the center of the wake as defined from flow photographs such as figure 28:

$$\frac{x}{D} = \frac{1}{4} \left( \frac{V}{V_j} \right)^2 \left( \frac{-z}{D} \right)^3 \sec^2 \theta_j + \left( \frac{-z}{D} \right) \tan \theta_j \quad (16)$$

Margason then divided the wake into short segments aligned so as to approximate the actual wake curvature. A few initial results are presented in figure 29. The interference is again calculated for the model centered in a closed tunnel having a width-height ratio of 1.5. The initial direction of the jet is vertically downward ( $\theta_j = 0$ ) and the jet diameter is assumed to be one-fifth of the full height of the tunnel. Two cases are treated:  $V/V_j = 1/4$  and  $V/V_j = 1/2$ . The results are presented directly in terms of  $\Delta\alpha$  and  $q_c/q$ , and are compared with the corresponding values from reference 5 using both the original skew angle and the effective skew angle as previously defined. The distribution of  $\Delta\alpha$  and  $q_c/q$  over the longitudinal axis of the tunnel is shown.

It will be observed that, irregardless of the skew angle used, the straight line wake does not predict the proper distribution of interference along the longitudinal axis of the tunnel in the more severe case ( $V/V_j = 1/4$ ). On the other hand, for the more moderate condition of  $V/V_j = 1/2$ , the differences between the curved wake calculations and those of reference 5 using the effective skew angle are small. In the latter case, the use of reference 5 should provide adequate interference results. The conditions at  $V/V_j = 1/4$  are so severe that recirculation effects (to be discussed subsequently) would undoubtedly occur and neither system would be usable for other reasons. Provided that model sizes, loadings, and velocities are held to limits chosen to avoid recirculation effects, it would appear that the interference theory of reference 5 should be adequate provided that the effective skew angle is used.

## REPRESENTATION OF THE GROUND

The V/STOL aircraft which have already flown have exhibited a wide variety of powerful ground effects, ranging from increased lift for helicopters to premature stall and large decreases in control effectiveness for tilt-wing and deflected slipstream types. The size and unpredictability of these ground effects has led to greatly increased emphasis on wind-tunnel tests in ground effect.

Wind-tunnel ground-effect tests run on V/STOL models can be deceptive if special precautions are not taken. The ground plane or the tunnel floor which may be used to represent the ground in the tunnel is not necessarily a valid representation (ref. 24). The model moving in still air over the ground is in a flow with no boundary layer at the ground; however, when the air is moved over the stationary model and the stationary ground plane in the tunnel, a substantial boundary layer may exist at the ground plane. A schematic picture of the two flows for a jet-flap model is shown in figure 30. In the case of a moving model, the jet sheet creates a small disturbance at its intersection with the ground and then flows rearward. When only the air moves, as in the wind tunnel, the disturbance caused by the jet sheet impinging on the ground is propagated forward in the low energy air of the boundary layer causing significant changes in the entire flow field.

Numerous schemes of "image models," boundary-layer suction, and blowing at the ground plane have been proposed to eliminate the unwanted boundary-layer effects. In practice, the use of some of these systems might require significant research programs in order to determine the proper distribution of suction or blowing for each configuration and test condition. Too much could be equally as bad as too little.

The most successful method used to date is the use of a moving or endless-belt ground plane (ref. 25). The proper matching is essentially ensured provided that the belt speed is identical to the tunnel velocity and provided that the boundary layer at the start of the belt is removed by a suction slot.

Figure 31 presents data from reference 25 indicating those regions where the use of a moving belt has been shown to be necessary when testing full-span, high-lift models. With the belt stationary, the lift-curve changes slope abruptly at some angle of attack as indicated by the small sketch on figure 31. Below this point, the data are essentially identical irregardless of whether or not the belt is moving. The point of divergence is taken as the criterion.

Figure 31 shows clearly that there is an essentially linear relationship between the lift coefficient above which the moving belt is required and  $h/b$  (where  $b$  is now the full wing span). It transpires that this combination of height and lift coefficient is such that the theoretical wake always impinges at a fixed number of wing spans behind the model. If the effective wake skew angle is used, the appropriate distance is  $2-1/2$  spans; if the original momentum skew angle is used, the appropriate distance is one span. Extrapolation of this simple rule would indicate that, if the model span and lift coefficient are

sufficiently great, a moving belt floor may be required even when attempting to obtain out-of-ground effect data with the model centered in the wind tunnel.

Some difficulties in the use of a belt should be noted. There is a tendency for the belt to lift off its bed under test conditions. Suction between the belt and its bed is indicated as a means of overcoming this problem. It cannot be completely overcome if the wake is sufficiently strong. In one recent test of a lift-jet model in the Langley 17-foot test section, the jets pushed the belt down against the bed in the center of the belt; however, the belt was lifted on each side of the central depression. In a case like this, the measured characteristics are more nearly like those for the model flying down the axis of a valley-like depression.

### RECIRCULATION LIMITS

One of the most significant recent developments in V/STOL testing techniques has been the discovery, by Rae (ref. 26) at the University of Washington, of limits to the minimum speed at which high-lift tests can be run successfully in a wind tunnel. The physical problem can be explained by examining figure 32.

The wake leaving a lifting model is, of course, deflected downward. Eventually it approaches the floor. Then moving under the combined effects of itself and the floor, it moves outward approaching the walls. Upon nearing the walls, the wake path proceeds upward and then, upon nearing the ceiling, inward. Near the center of the ceiling the rejoining portions of the wake again pass downward. Under normal conditions, this recirculation pattern is established at distances well down the diffuser and persists until broken up by the action of turning vanes, fan, straighteners, screens, honeycombs, and the settling chamber. If the contraction ratio is very low, some portion of the wake, if only a region of altered dynamic pressure may persist even back through the test section.

If the wake is sufficiently strong, it is deflected more sharply, and the recirculation pattern moves forward closer to the model. Eventually conditions become sufficiently severe that the recirculation actually envelops the model. At, or near, this point the flow in the tunnel no longer represents free air and data taken under such conditions is invalid and should be disregarded.

As it turns out, the onset of recirculation can also be estimated from the calculated impingement point of the wake on the floor. There is insufficient evidence, as yet, to make a clear choice as to whether this comparison should be made on a basis of momentum skew angle or effective skew. The tests to date indicate that either skew angle will suffice, although the numbers used as limiting values will naturally depend upon which angle is chosen. The limiting values for closed wind tunnels are shown in figure 33 as calculated with the momentum skew angle.

Note that the limits are a function of the wind-tunnel proportions or rectangularity. It seems to make little difference whether the tunnel is deep or wide just so the proportions remain the same. It will also be noted that fillets worsen the situation some. Qualitatively, it seems that those tunnels which

differ most from circular are superior. This result might be anticipated since it is obviously easiest to start a circulatory motion of this type in a circular tunnel.

For tunnels of equal area, decreasing width-height ratio leads to a greater distance between the model and the floor, and therefore, for a given wake angle, a longer distance downstream to the impingement point. Thus a deeper tunnel will allow testing to a lower skew angle and, consequently, a lower forward speed. On the other hand, for a given tunnel area and a given model span, the narrow deep tunnel will produce more pronounced nonuniformity across the span. Considering these effects as well as the variation of limit distance in figure 33, it would appear that a width-height ratio on the order of 1.25 is probably desirable for V/STOL testing.

The nature of the recirculation limit is such that some relief may be obtained by moving the model above center and thus further from the floor. The extent of this relief will be limited, however, by changes in wall interference and by an increased tendency toward separation of the tunnel flow from the ceiling.

#### ADEQUACY OF STEADY-STATE TESTS

Many problems associated with wind-tunnel testing remain to be answered. Some are fairly fundamental; of these, one will be pointed out herein.

Transition testing of a V/STOL model consists of setting up and running a series of fixed steady-state flight conditions in the tunnel following an appropriate schedule of configuration variables, power, angle of attack, and tunnel velocity. It is tacitly assumed that these steady-state conditions can then be used to obtain the instantaneous values achieved by the aircraft as it passes through a continuous sequence in transition.

This quasi-static approach is probably adequate for an aircraft making a very long slow transition from forward flight to hovering. On the other hand, the extreme rate of fuel consumption of some types of aircraft when the lift is supplied directly by the engines dictates an extremely rapid transition period. On some jet-lift types, it may be necessary to incur velocity changes in excess of 100 knots, and angle-of-attack changes on the order of  $10^\circ$  to  $20^\circ$ , in a period of only 10 or 15 seconds if the operation is to be conducted in an economic manner.

Figure 34 presents some very old data (ref. 27) showing the effect of rate of change of angle of attack on the lift curve of a simple airplane at low speed. Very small  $d\alpha/dt$  changes are seen to produce disproportionately large differences in both the maximum lift coefficient and the angle at which it occurs. The rates of change in some V/STOL transitions may be an order of magnitude greater than those of figure 34, and consequently, larger effects might be expected.

It would seem that an effect as potentially as significant as this should be investigated experimentally for several configurations. The results of such an investigation might well indicate a need for tunnels capable of reproducing a variety of rates of change of both angle of attack and tunnel velocity, both independently and in combination.

#### CONCLUDING REMARKS

Experimental results indicate the possibility of very large wall interference in V/STOL wind-tunnel tests. In some cases, the wall interference may be sufficiently great to reverse even the trends of the parameters under investigation.

Considerable care is required in applying wall interference corrections to V/STOL data. The interference factors needed are affected not only by the type of tunnels and its proportions, but also by effective skew angle, span of both lifting system and tail, configuration, model location, tail length and height, angle of attack, the relationship between the effective pivot point and the aerodynamic center, and the c.g. position. The effect of these variables can be obtained from the theory of NASA TR R-124 by the use of superposition techniques; the optimum procedure being to accomplish the superposition directly within a computer.

In the case of many complex and multielement models, it is necessary to know the contribution of the individual elements of the model to the overall forces in order to apply corrections in a reasonable and proper manner. The use of auxiliary balances to obtain this information is indicated.

Even after accounting for the aforementioned features, discrepancies may remain as a result of the nonuniformity of interference over the extent of the model. These discrepancies are largely the result of an imperfect understanding of the aerodynamics of most V/STOL configurations. If adequate theories existed, it would be possible to remove such effects from the data. Simple equivalence concepts, however, can indicate the order of magnitude of some of these effects.

The floor of the wind tunnel deserves particular attention particularly for tests of large models at extreme lift coefficients and for ground-effect testing. The boundary layer on the floor may substantially affect the data. Removal or elimination of the boundary layer during such tests is indicated.

Recirculation of the flow within the tunnel results in limits to the minimum speed (or skew angle) at which V/STOL tests can be accomplished successfully. Some relief can be obtained by proper choice of tunnel configuration. Some relief can also be obtained by moving the model to an above center position in the tunnel; however, the extent of this gain is limited by effects on wall interference and by an increased tendency toward separation of the tunnel flow from the ceiling.

Many questions concerning V/STOL wind-tunnel technique remain to be answered. For example, rates of change of angle of attack, an order of magnitude less than those experienced in some V/STOL transitions, are known to produce significant effects on wind-tunnel data. The investigation of effects such as these is indicated.

## REFERENCES

1. Kuhn, Richard E.; and Naeseth, Rodger L.: Tunnel-Wall Effects Associated With VTOL-STOL Model Testing. AGARD Report 303, 1959.
2. Prandtl, L.: and Tietgens, O. G. (J. P. Den Hartog, Trans.): Applied Hydro- and Aeromechanics. Dover Pub., Inc., 1957, pp. 222-225.
3. Glauert, H.: The Interference of Wind Channel Walls on the Aerodynamic Characteristics of an Aerofoil. R & M No. 867, Brit. A.R.C., 1923.
4. Theodorsen, Theodore: The Theory of Wind-Tunnel Wall Interference. NACA Rept. 410, 1931.
5. Heyson, Harry H.: Linearized Theory of Wind-Tunnel Jet-Boundary Corrections and Ground Effect for VTOL-STOL Models. NASA TR R-124, 1962.
6. Lee, Jerry Louis: An Experimental Investigation of the Use of Test Section Inserts as a Device to Verify Theoretical Wall Corrections for a Lifting Rotor Centered in a Closed Rectangular Test Section. M.S. Thesis, Univ. of Washington, Aug. 20, 1964.
7. Davenport, Edwin E.; and Kuhn, Richard E.: Wind-Tunnel-Wall Effects and Scale Effects on a VTOL Configuration with a Fan Mounted in the Fuselage. NASA TN D-2560, 1965.
8. Grunwald, Kalman J.: Experimental Study of Wall Effects and Wall Corrections for a General-Research V/STOL Tilt-Wing Model With Flap. NASA TN D-2887, 1965.
9. Staff of Powered-Lift Aerodynamics Section, NASA Langley Research Center: Wall Effects and Scale Effects in V/STOL Model Testing. AIAA Aerodynamic Testing Conf., March 1964, pp. 8-16.
10. Heyson, Harry H.; and Grunwald, Kalman J.: Wind-Tunnel Boundary Interference for V/STOL Testing. Conference on V/STOL and STOL Aircraft, NASA SP-116, 1966, pp. 409-434.
11. Eldridge, W. M. : An Evaluation of Wall Interference Effects and Test Limits for a Jet-Lift V/STOL Wind-Tunnel Model. Rept. No. D6-15021 TN, Boeing Co., Airplane Division, 1966. (Proprietary)
12. Heyson, Harry H.: Nomographic Solution of the Momentum Equations for VTOL-STOL Aircraft. NASA TN D-814, 1961. (Also available as "V/STOL Momentum Equation," Space/Aero., Vol. 38, No. 2, July 1962, pp. B-18 to B-20.)
13. Heyson, Harry H.; and Katzoff, S.: Induced Velocities Near a Lifting Rotor With Nonuniform Disk Loading. NACA Rept. 1319, 1957. (Supersedes NACA TN 3690 by Heyson and Katzoff and TN 3691 by Heyson.)

14. Heyson, Harry H.: Tables of Interference Factors for Use in Wind-Tunnel and Ground-Effect Calculations for VTOL-STOL Aircraft. Part I - Wind Tunnels Having Width-Height Ratio of 2.0. NASA TN D-933, 1962.
15. Heyson, Harry H.: Tables of Interference Factors for Use in Wind-Tunnel and Ground-Effect Calculations for VTOL-STOL Aircraft. Part II - Wind Tunnels Having Width-Height Ratios of 1.5. NASA TN D-934, 1962.
16. Heyson, Harry H.: Tables of Interference Factors for Use in Wind-Tunnel and Ground-Effect Calculations for VTOL-STOL Aircraft. Part III - Wind Tunnels Having Width-Height Ratio of 1.0. NASA TN D-935, 1962.
17. Heyson, Harry H.: Tables of Interference Factors for Use in Wind-Tunnel and Ground-Effect Calculations for VTOL-STOL Aircraft. Part IV - Wind Tunnels Having Width-Height Ratio of 0.5. NASA TN D-936, 1962.
18. Heyson, Harry H.: Tables of Interference Factors for Use in Correcting Data From VTOL Models in Wind Tunnels With 7 by 10 Proportions. NASA SP-3039, 1967.
19. Glauert, H.; and Hartshorn, A. S.: The Interference of Wind Channel Walls on the Downwash Angle and the Tailsetting to Trim. R & M No. 947, Brit. A. R. C., 1925.
20. Heyson, Harry H.: Equations for the Application of Wind-Tunnel Wall Corrections to Pitching Moments Caused by the Tail of an Aircraft Model. NASA TN D-3738, 1966.
21. Wheatley, John B.: An Aerodynamic Analysis of the Autogyro Rotor With a Comparison Between Calculated and Experimental Results. NACA Rept. 487, 1934.
22. Sweet, George E.: Static Stability Measurements of a Stand-On Type Helicopter With Rigid Blades Including a Comparison With Theory. NASA TN D-189, 1960.
23. Heyson, Harry H.: Wind-Tunnel Wall Effects at Extreme Force Coefficients. Presented at the International Congress of Subsonic Aeronautics (New York Academy of Sciences), New York, New York, April 3-6, 1967. (Available from NASA as TM X-59742.)
24. Werlé, Henri: Simulation of de L'Effet de Sol au Tunnel Hydrodynamique (Ground-Effect Simulation at the Water-Tunnel). La Rech. Aérospatiale, no. 95, July-Aug. 1963, pp. 7-15.
25. Turner, Thomas R.: Endless-Belt Technique for Ground Simulation. Conference on V/STOL and STOL Aircraft, NASA SP-116, 1966, pp. 435-446.

26. Rae, William H., Jr.: Limits on Minimum-Speed V/STOL Wind-Tunnel Tests. Jour. of Aircraft, Vol. 4, No. 3, May-June, 1967, pp. 249-254. (Supersedes AIAA Paper No. 66-736, 1966.)
27. Silverstein, Abe; Katzoff, S.; and Hootman, James A.: Comparative Flight and Full-Scale Wind-Tunnel Measurements of the Maximum Lift of an Airplane. NACA Rept. 618, 1938.

ASSUMED WAKE

CLASSICAL THEORY

NASA TR R-124

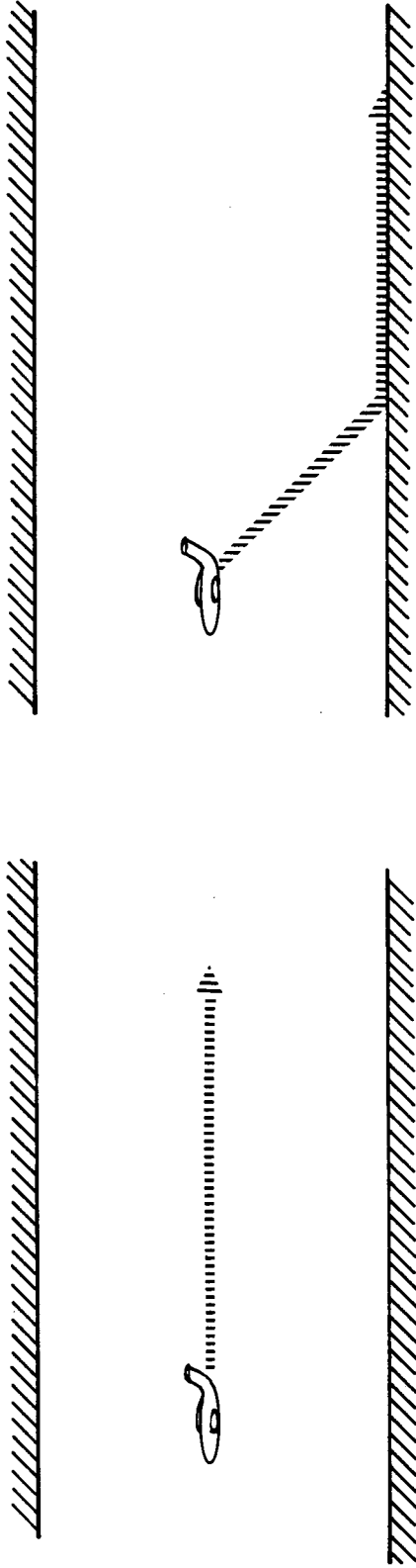


Figure 1.- Comparison of wake shapes assumed in classical theory and in reference 5.

$$\frac{B}{H} = 1.5$$

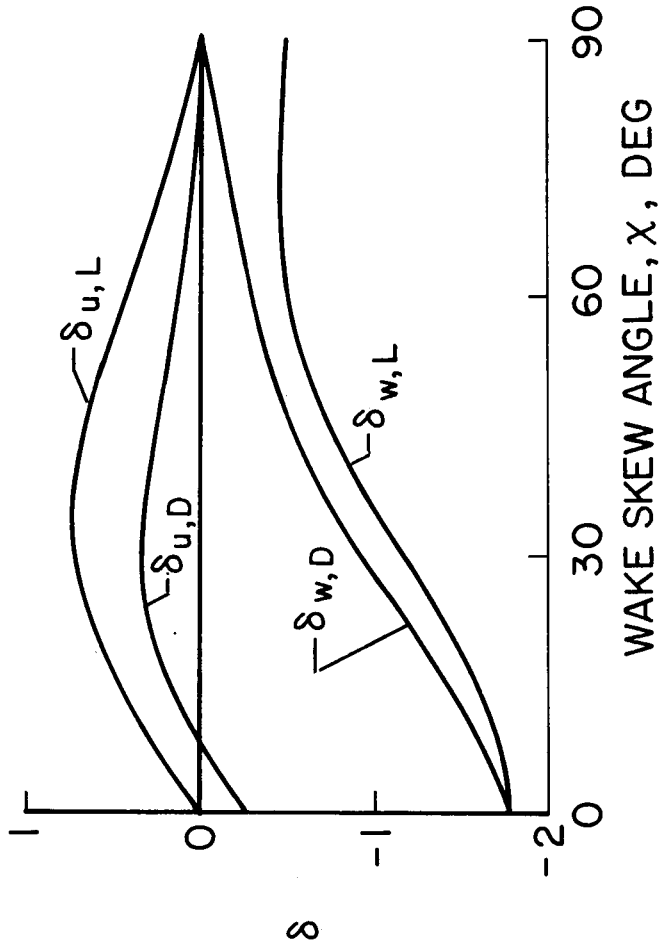
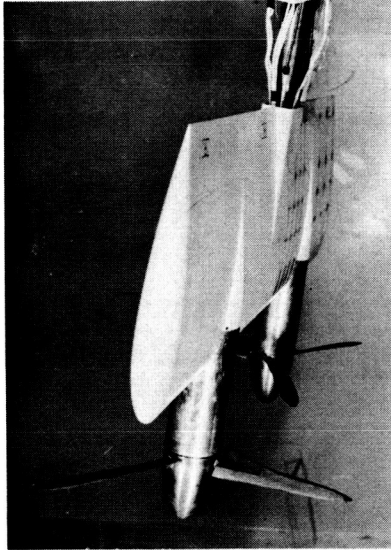
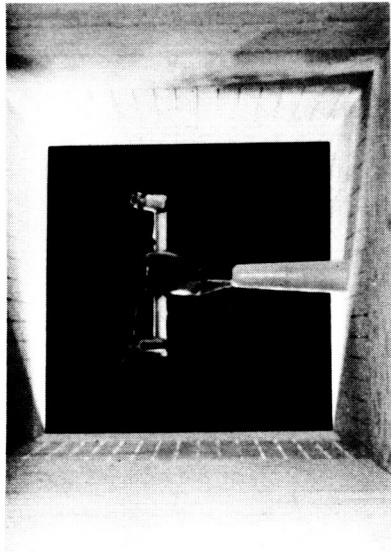


Figure 2.- Interference factors at the center of lift for a vanishingly small model centered in a closed rectangular tunnel.

TILT WING

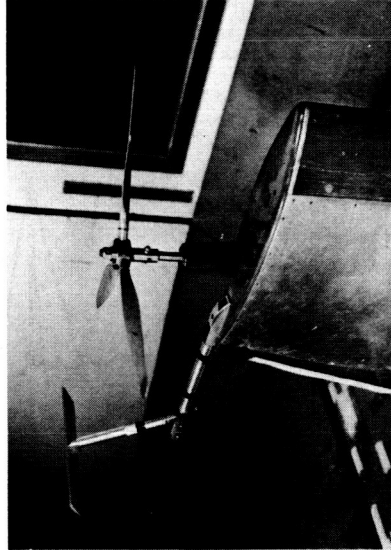
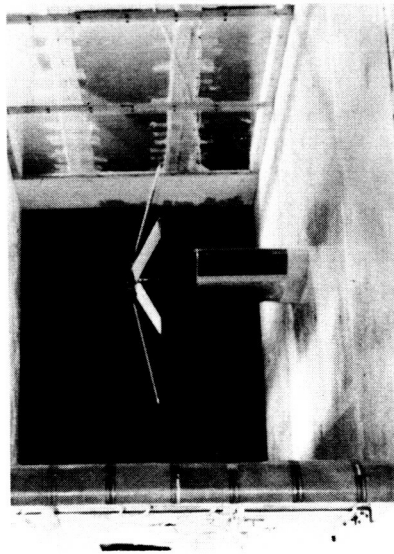


NRC

LANGLEY

ROTOR

LIFTING PROPELLER

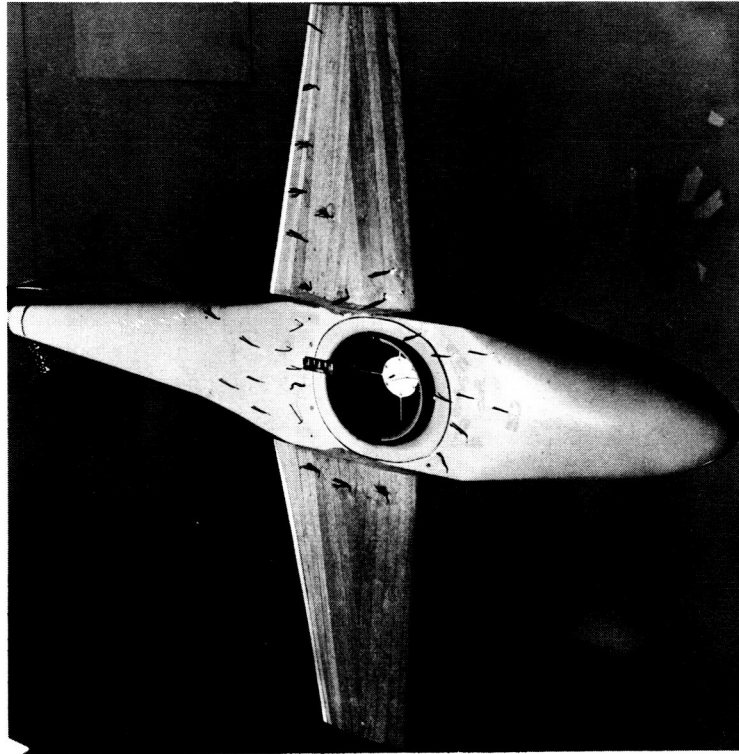


UNIVERSITY OF WASHINGTON

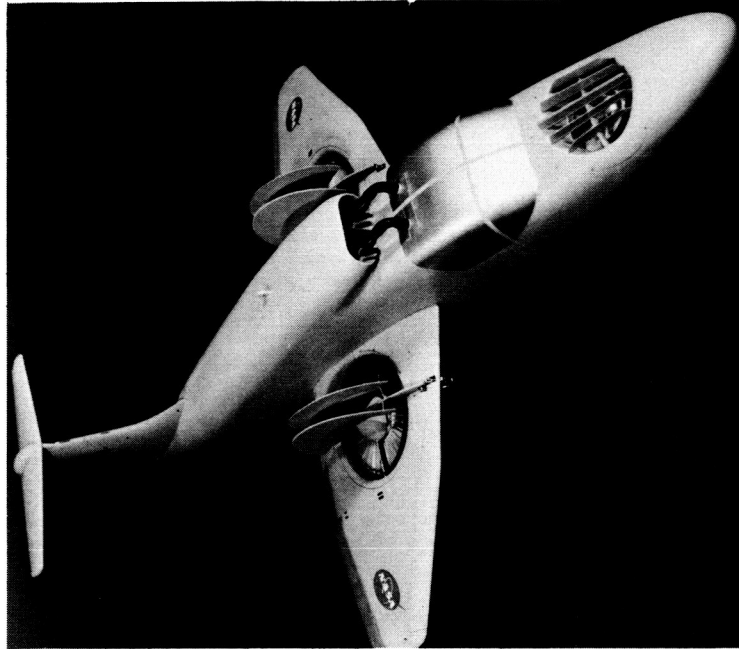
Figure 3.- Tilt-wing, rotor, and lifting propeller models tested in verifying the theory of reference 5.

## LIFTING-FAN MODELS

FAN IN FUSELAGE



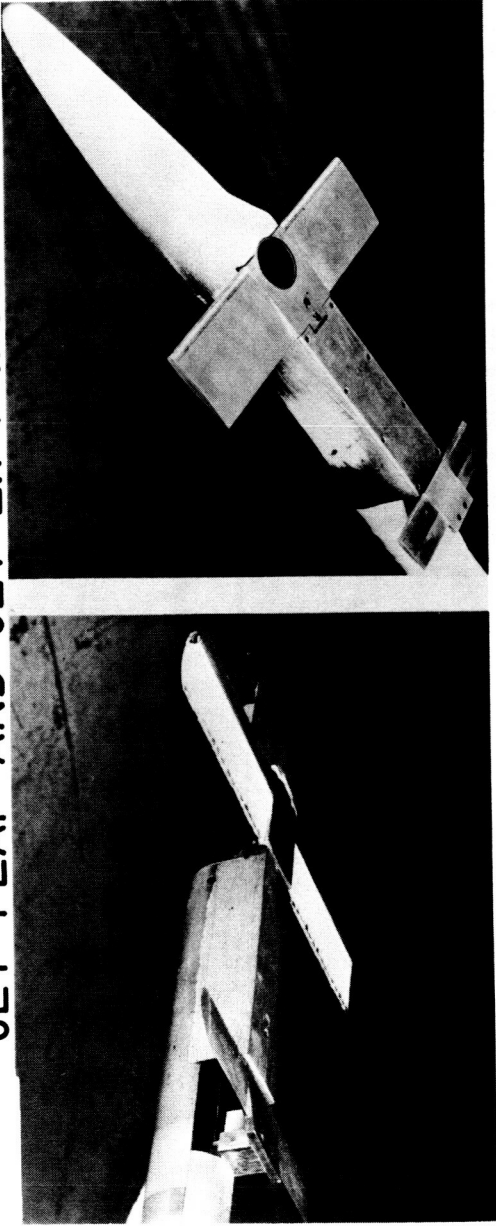
FAN IN WING



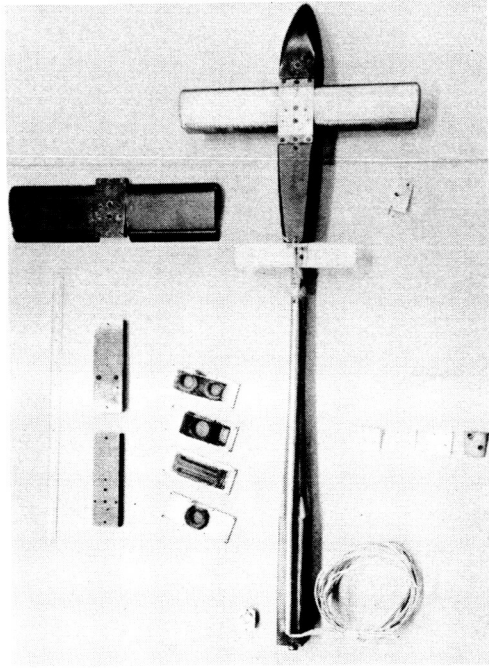
LANGLEY

Figure 4.- Lift-fan models tested in verifying the theory of reference 5.

# JET-FLAP AND JET-LIFT MODELS



LANGLEY



BOEING CO.

Figure 5.- Jet-flap and jet-lift models tested in verifying the theory of reference 5.

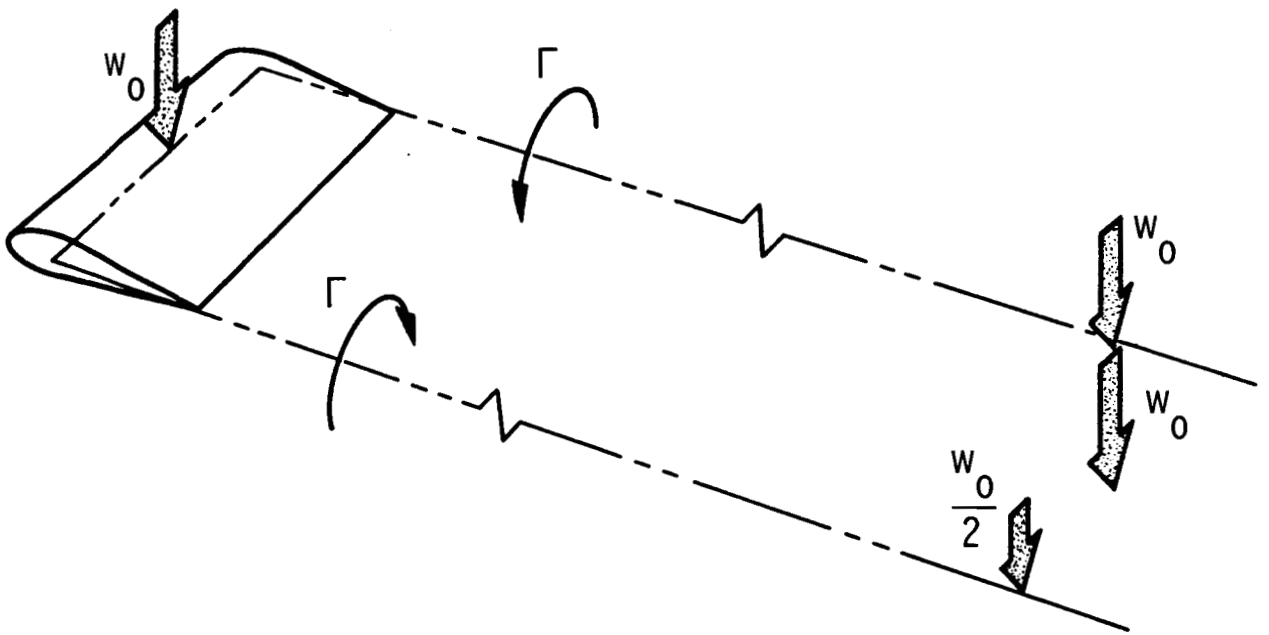


Figure 6.- Path of vorticity in the wake of a simple wing.

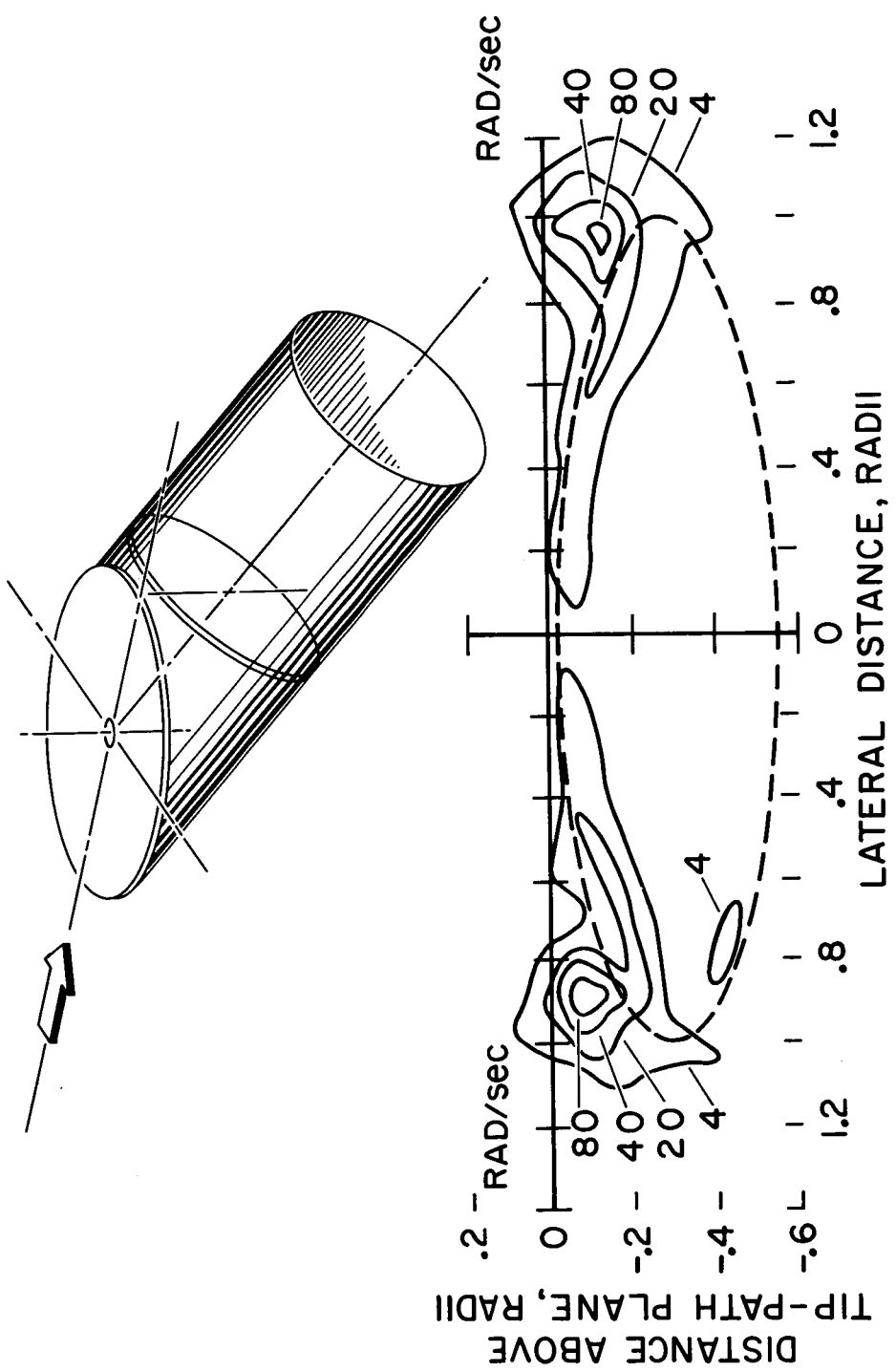


Figure 7.- Contours of equal value of vorticity measured 7 percent of a radius behind the trailing edge of a rotor.  $x = 75^\circ$ .

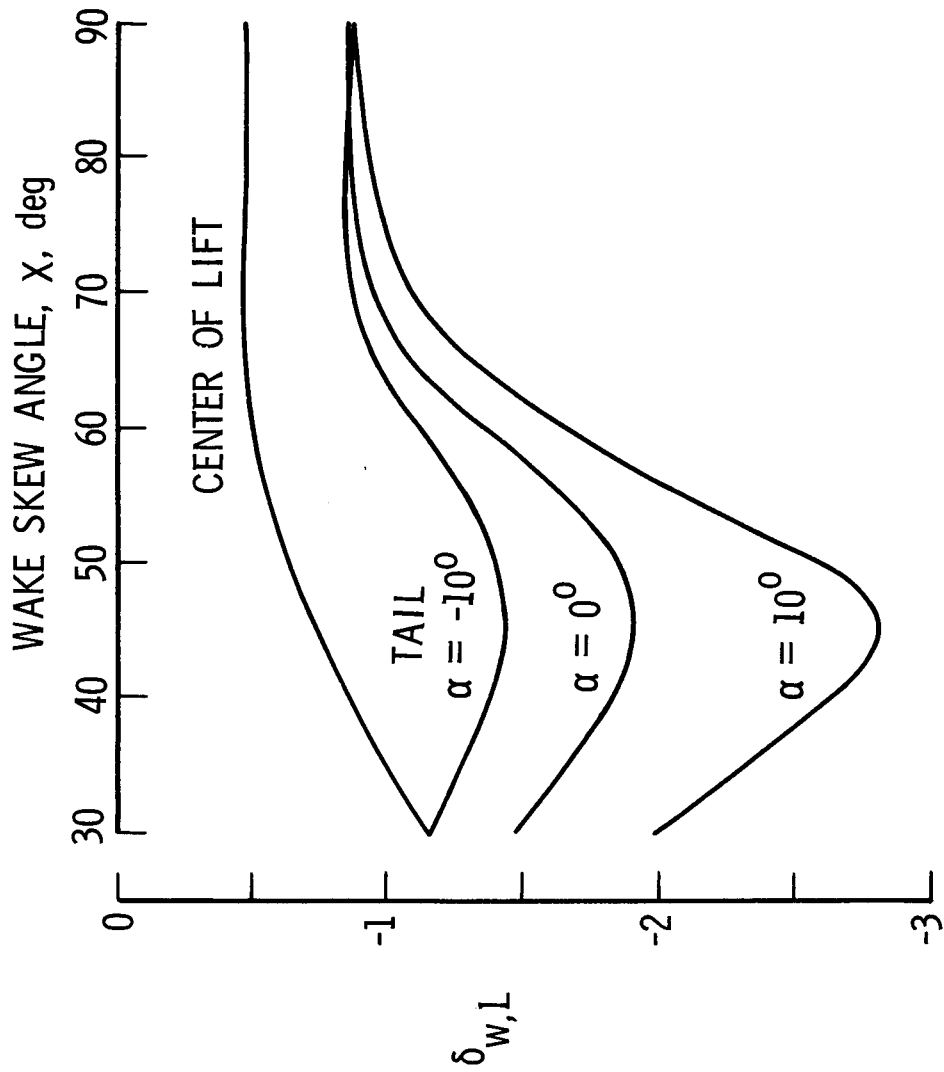


Figure 8.- Interference at a zero-span tail behind a vanishingly small model centered in a closed wind tunnel,  $\gamma = 1.5$ , tail length is one tunnel semiheight.

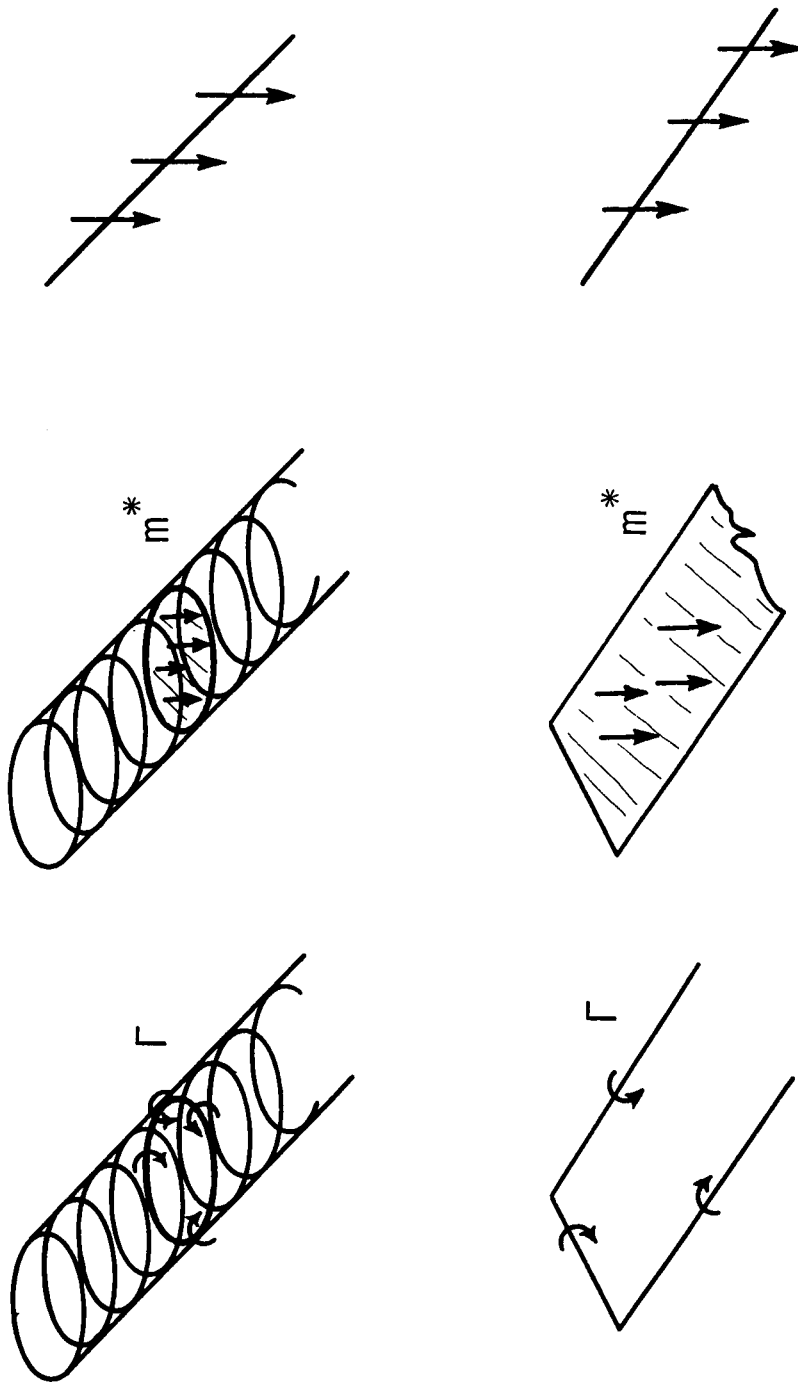


Figure 9.- Sketches illustrating reduction of idealized rotor and wing wakes into a semi-infinite string of point doublets.

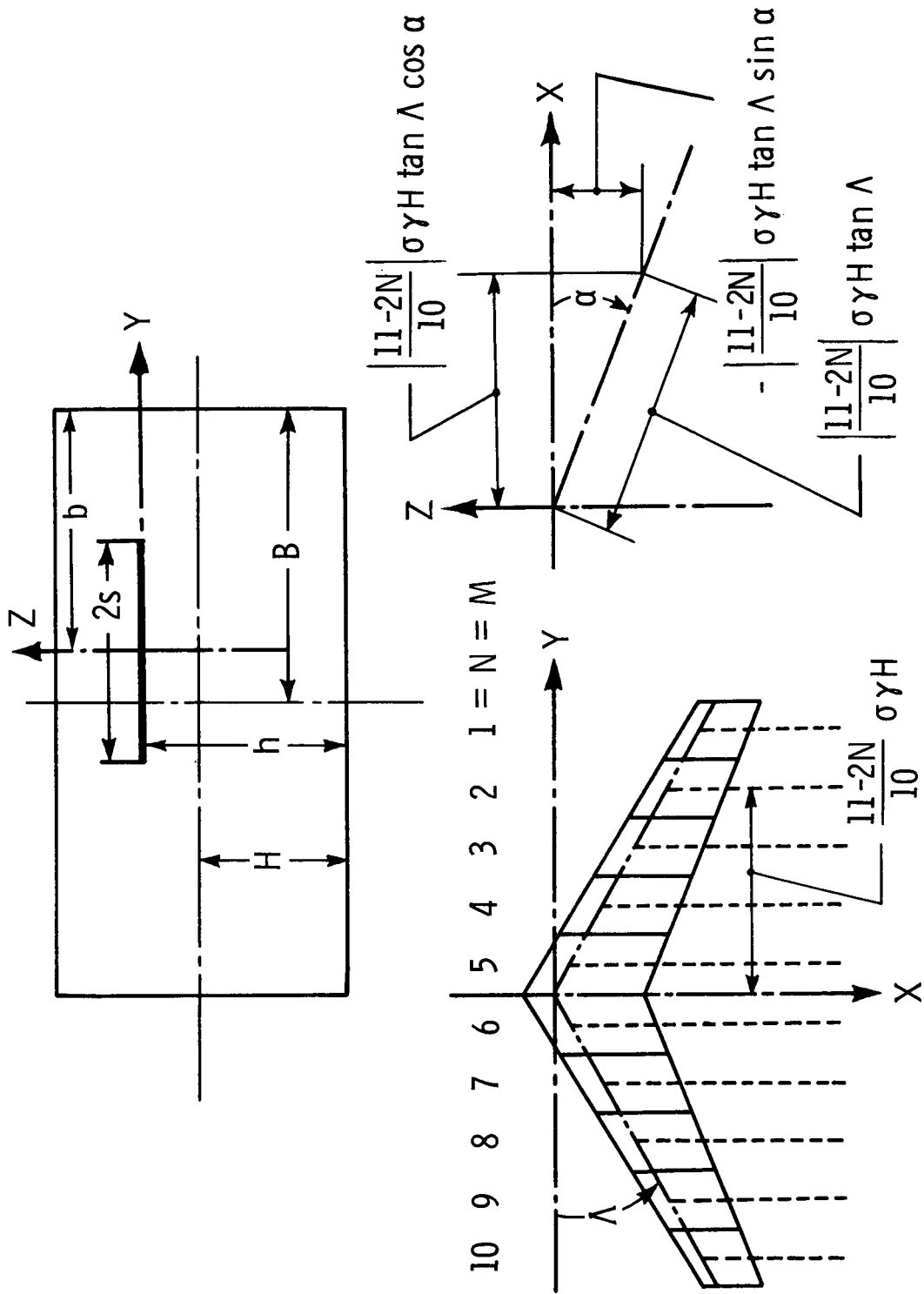


Figure 10.- Sketches illustrating the method of superposition in obtaining the correction factors for a swept wing of finite span.

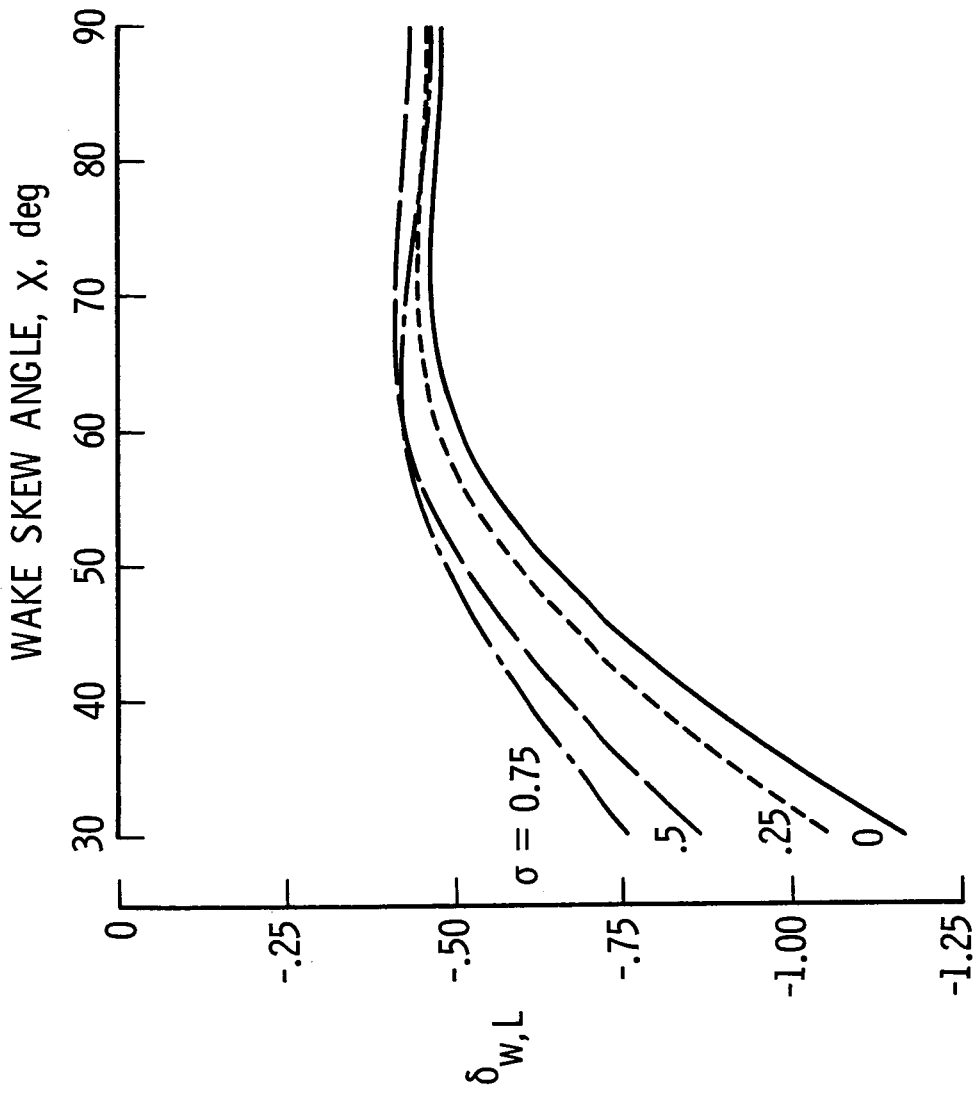


Figure 11.- Effect of span-width ratio on interference for a series of straight wings centered in a closed wind tunnel.  $\gamma = 1.5$ .

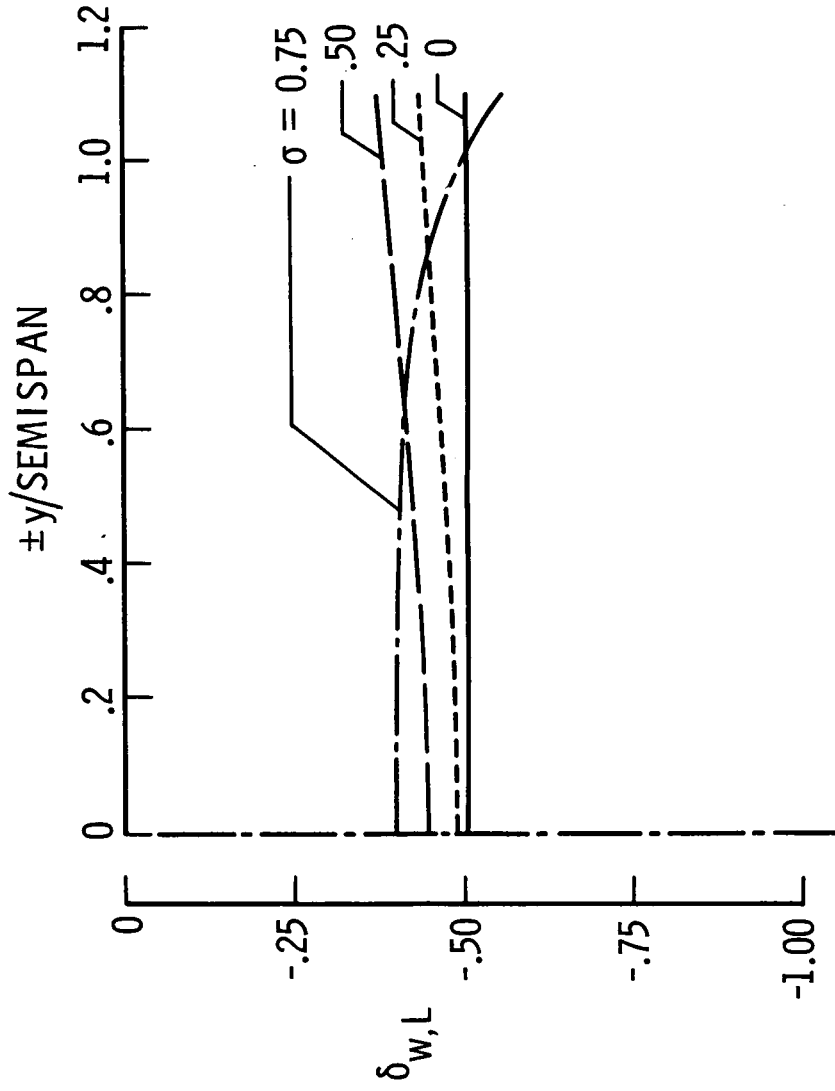


Figure 12.- Distribution of interference over the span for a series of straight wings centered in a closed wind tunnel.  $\gamma = 1.5$ ,  $x = 60^\circ$ .

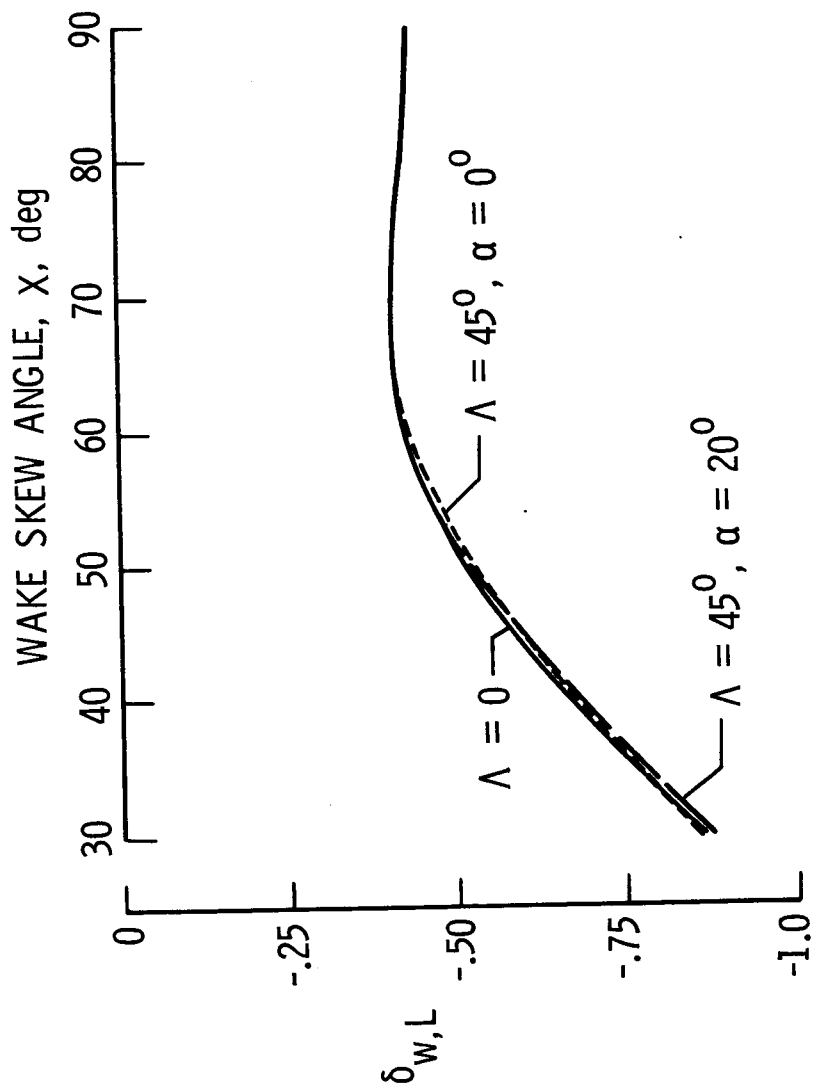


Figure 13.- Comparison of the average interference as affected by sweep and angle of attack for wings centered in a closed tunnel.  $\gamma = 1.5$ ,  $\sigma = 0.5$ .

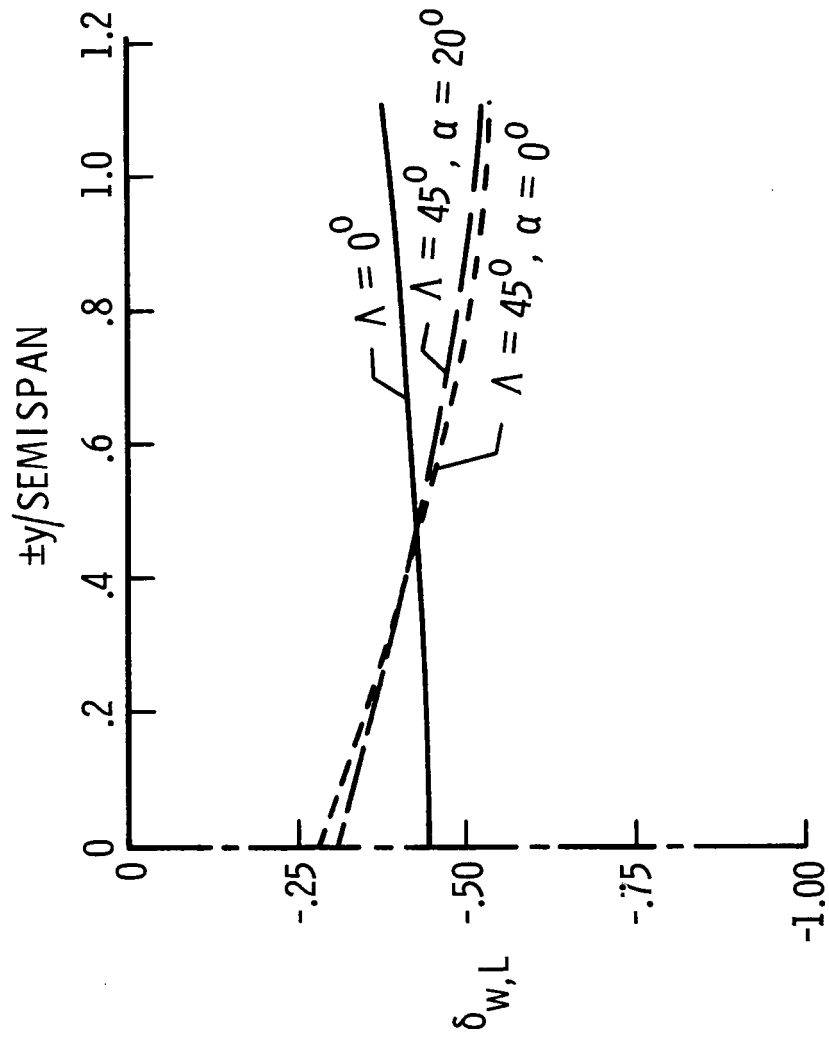


Figure 14.- Effect of sweep and angle of attack on the distribution of interference over the span of wings centered in a closed tunnel.  $\gamma = 1.5$ ,  $\sigma = 0.5$ ,  $x = 60^\circ$ .

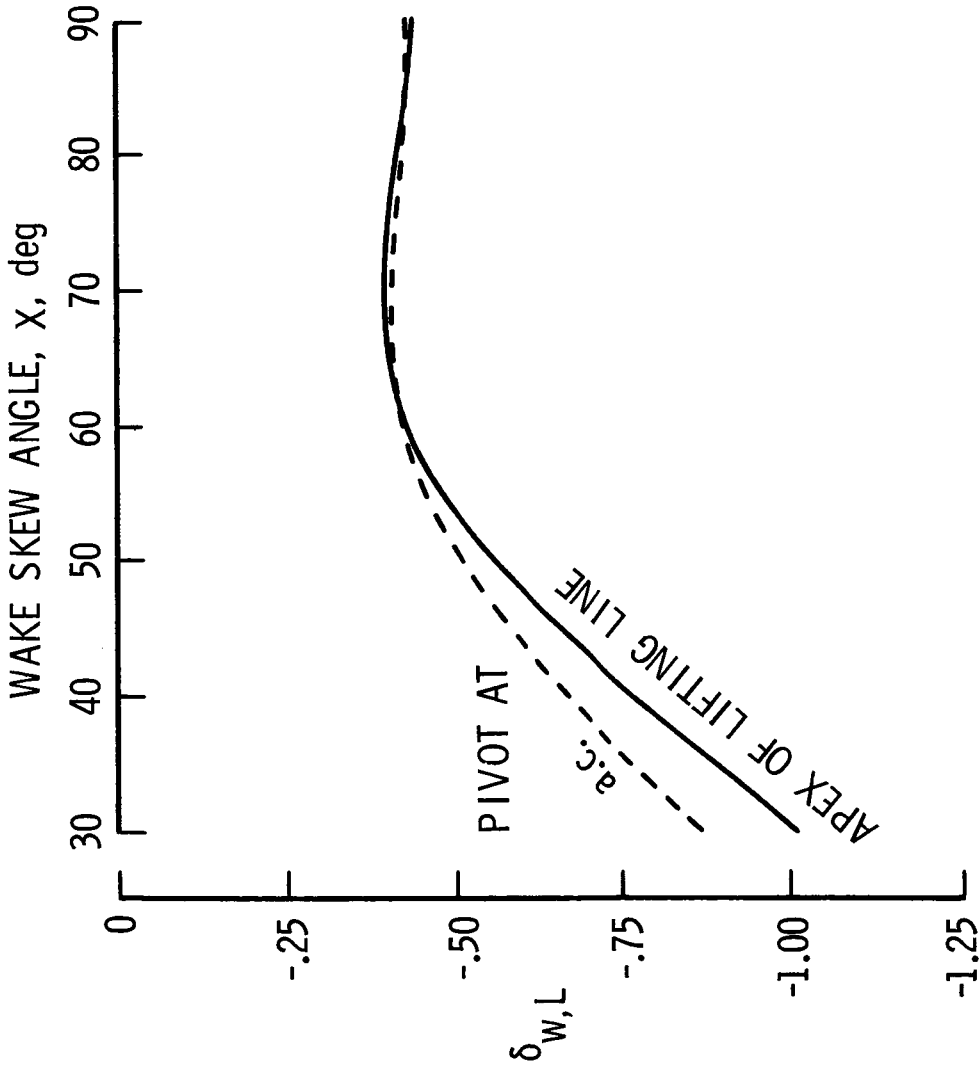


Figure 15.- Effect of pivot point location on the average interference of a swept wing ( $\Lambda = 45^\circ$ ) at  $\alpha = 20^\circ$  in a closed wind tunnel.  $\gamma = 1.5$ ,  $\sigma = 0.5$ .

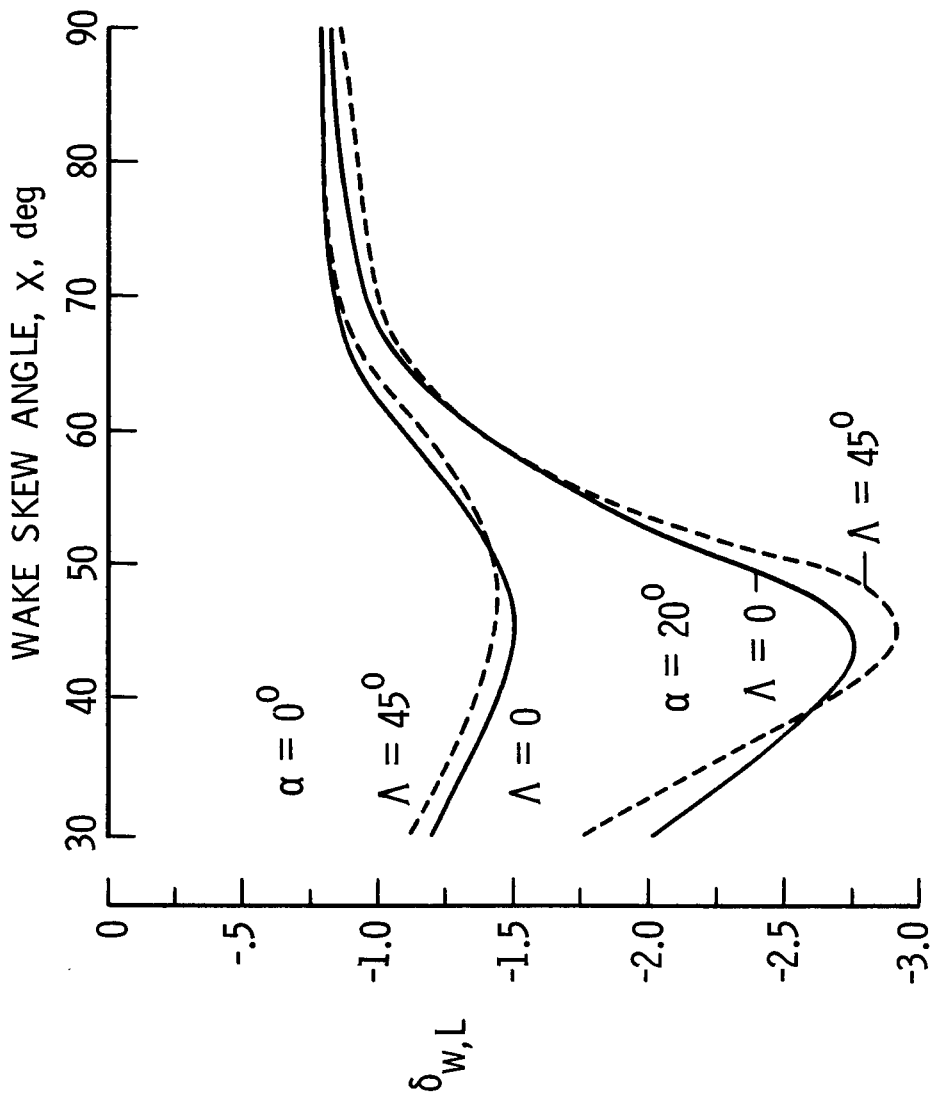


Figure 16.- Effect of sweep on the interference over a zero span tail behind a wing with aerodynamic center at the center of a closed wind tunnel.  $\gamma = 1.5$ ,  $\sigma = 0.5$ . Tail is two-thirds of wing span behind the aerodynamic center.

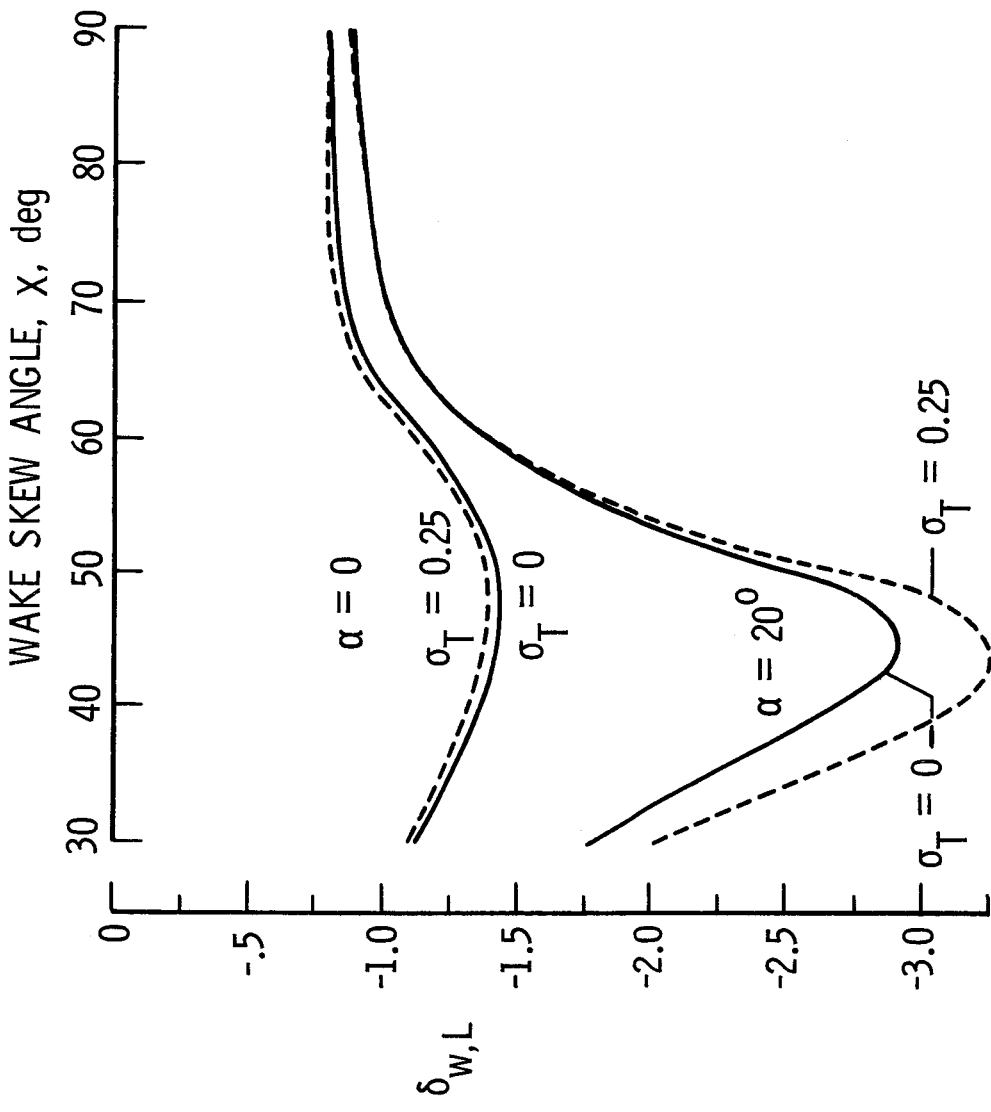


Figure 17.- Effect of tail span on the average interference over a tail behind a swept wing ( $\Lambda = 45^\circ$ ) centered in a closed wind tunnel.  $\gamma = 1.5$ ,  $\sigma = 0.5$ . Tail is two-thirds of wing span behind the aerodynamic center.

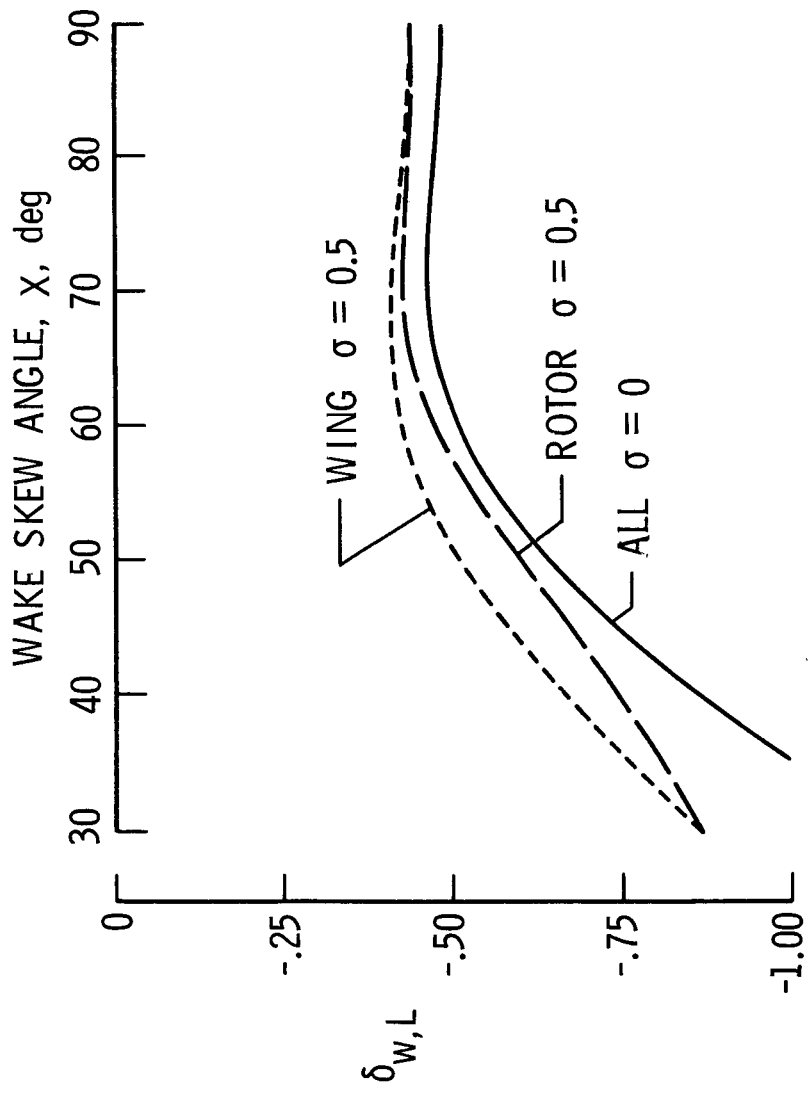


Figure 18.- Comparison of average interference over wings and rotors of equal span centered in a closed wind tunnel.  $\gamma = 1.5$ ,  $\alpha = 0^\circ$ .

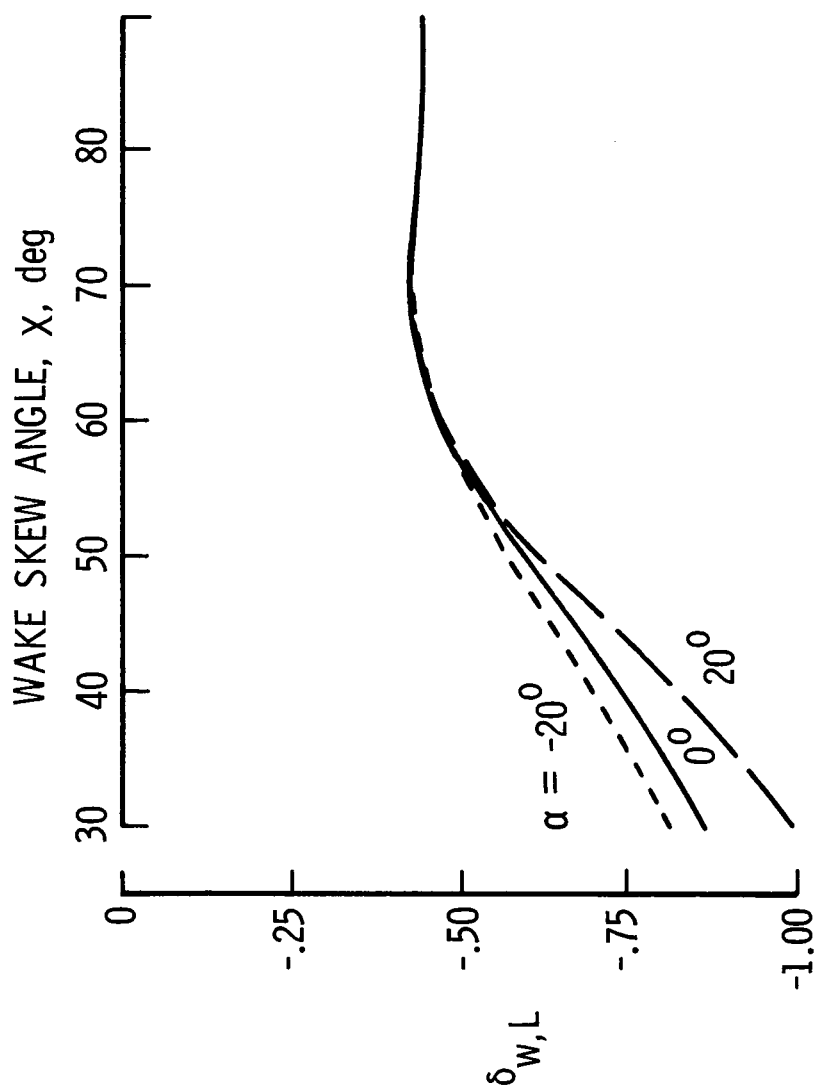


Figure 19.- Effect of angle of attack on the average interference over a rotor centered in a closed wind tunnel.  $\gamma = 1.5$ ,  $\sigma = 0.5$ .

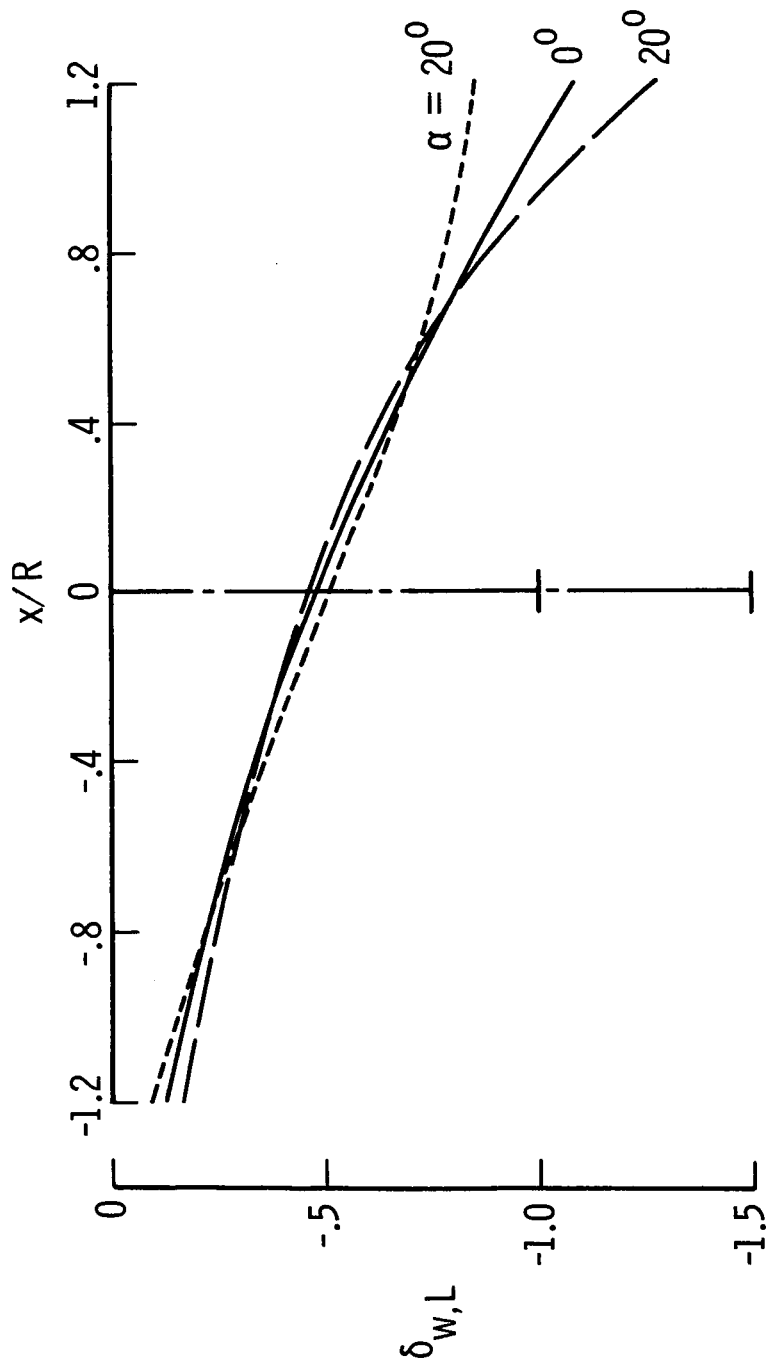
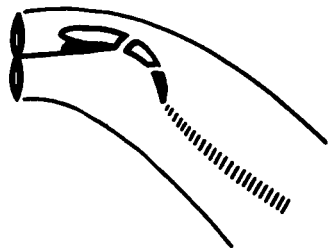
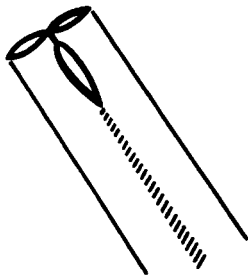


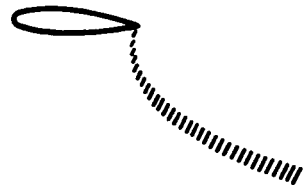
Figure 20.- Effect of angle of attack on the longitudinal distribution of interference over a rotor centered in a closed wind tunnel.  $\gamma = 1.5$ ,  $\sigma = 0.5$ ,  $x = 0.5$ ,  $x = 60^\circ$ .



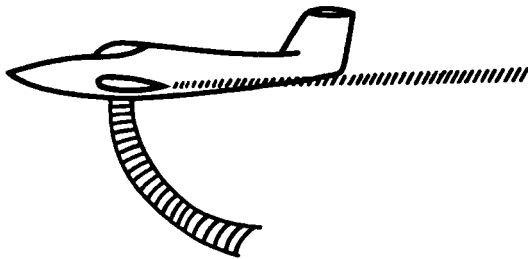
DEFLECTED SLIPSTREAM



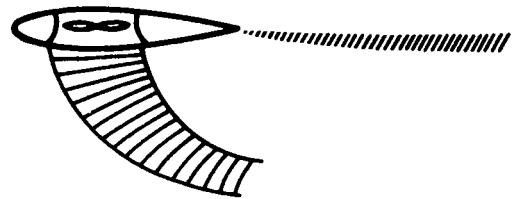
TILT WING



JET FLAP

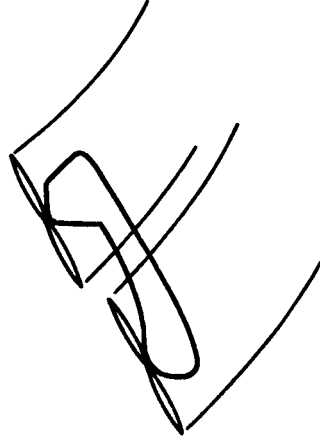


LIFT-JET



FAN-IN-WING

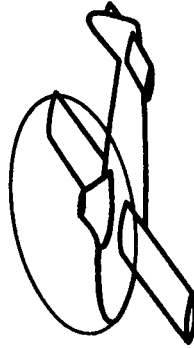
Figure 21.- Sketches illustrating complex types of V/STOL models.



TANDEM ROTOR



TILT ROTOR



UNLOADED ROTOR

Figure 22.- Sketches illustrating several types of multi-element V/STOL aircraft models.

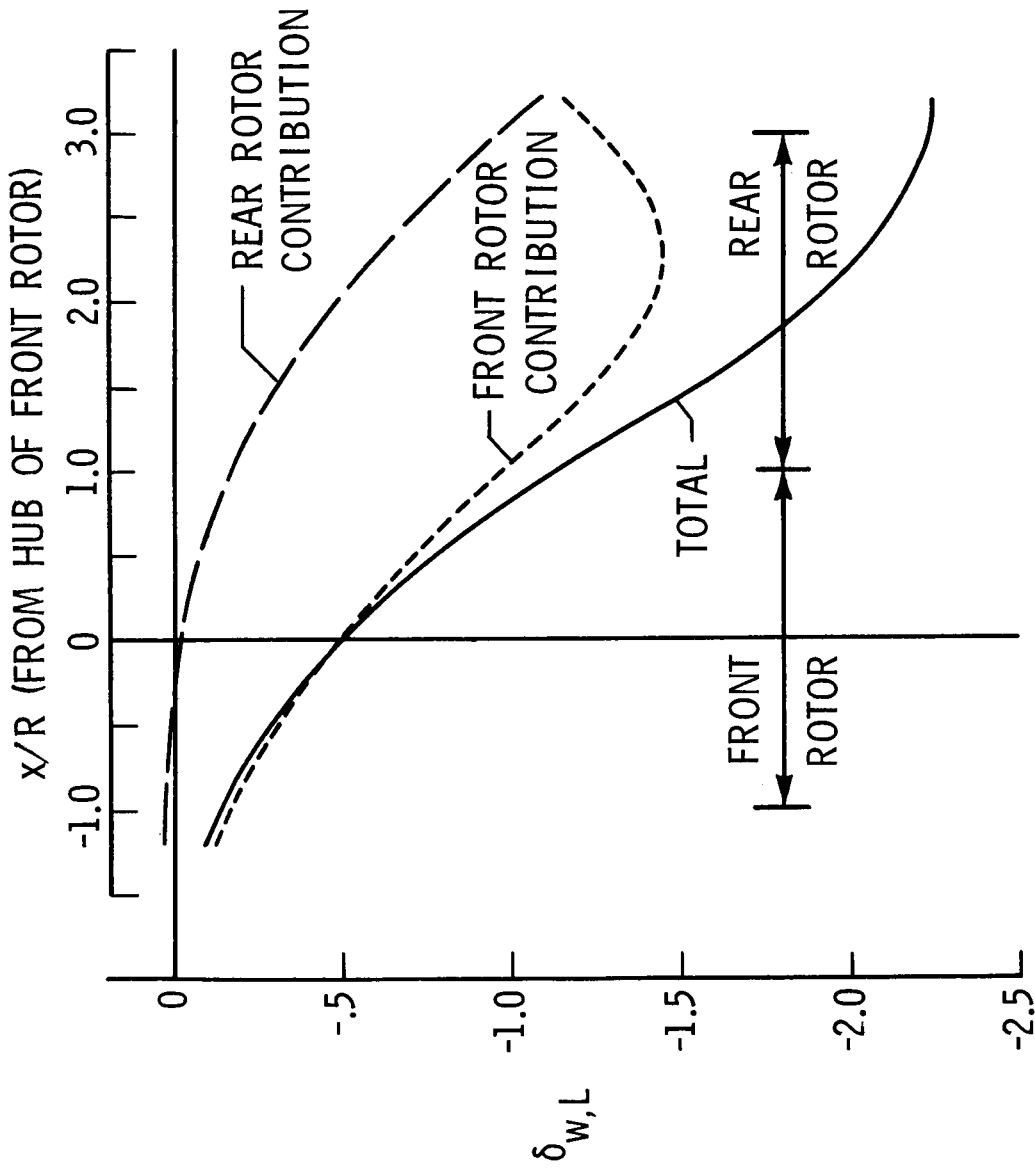


Figure 23.- Distribution of interference over the longitudinal axis of a tandem rotor system with the front rotor centered in a closed wind tunnel.  $\gamma = 1.5$ ,  $\sigma = 0.5$ ,  $\alpha = 0^\circ$ ,  $x = 60^\circ$ .

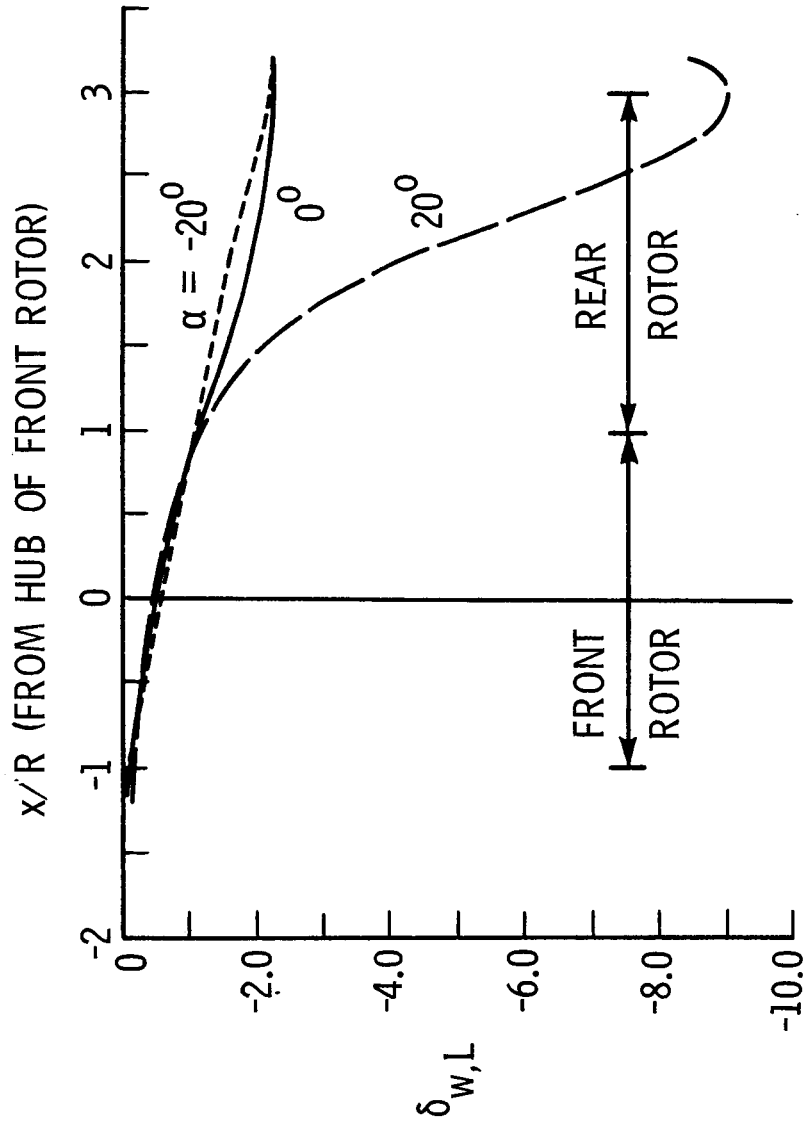


Figure 24.- Effect of angle of attack on the distribution of interference over the longitudinal axis of a tandem rotor system with the front rotor centered in a closed wind tunnel.  $\gamma = 1.5$ ,  $\sigma = 0.5$ ,  $x = 60^\circ$ .

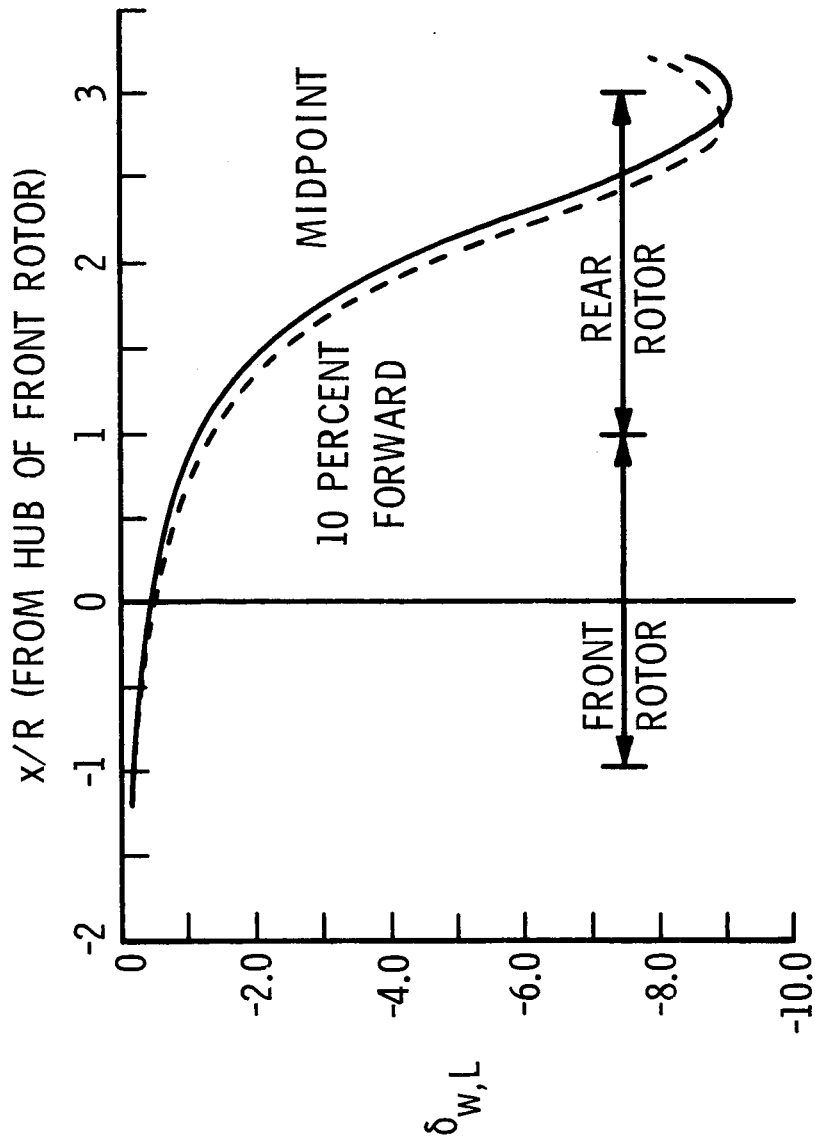


Figure 25.- Effect of center-of-gravity location on the distribution of interference over the longitudinal axis of a tandem rotor system with the front rotor centered in a closed wind tunnel.  $\gamma = 1.5$ ,  $\sigma = 0.5$ ,  $\alpha = 20^\circ$ ,  $x = 60^\circ$ .

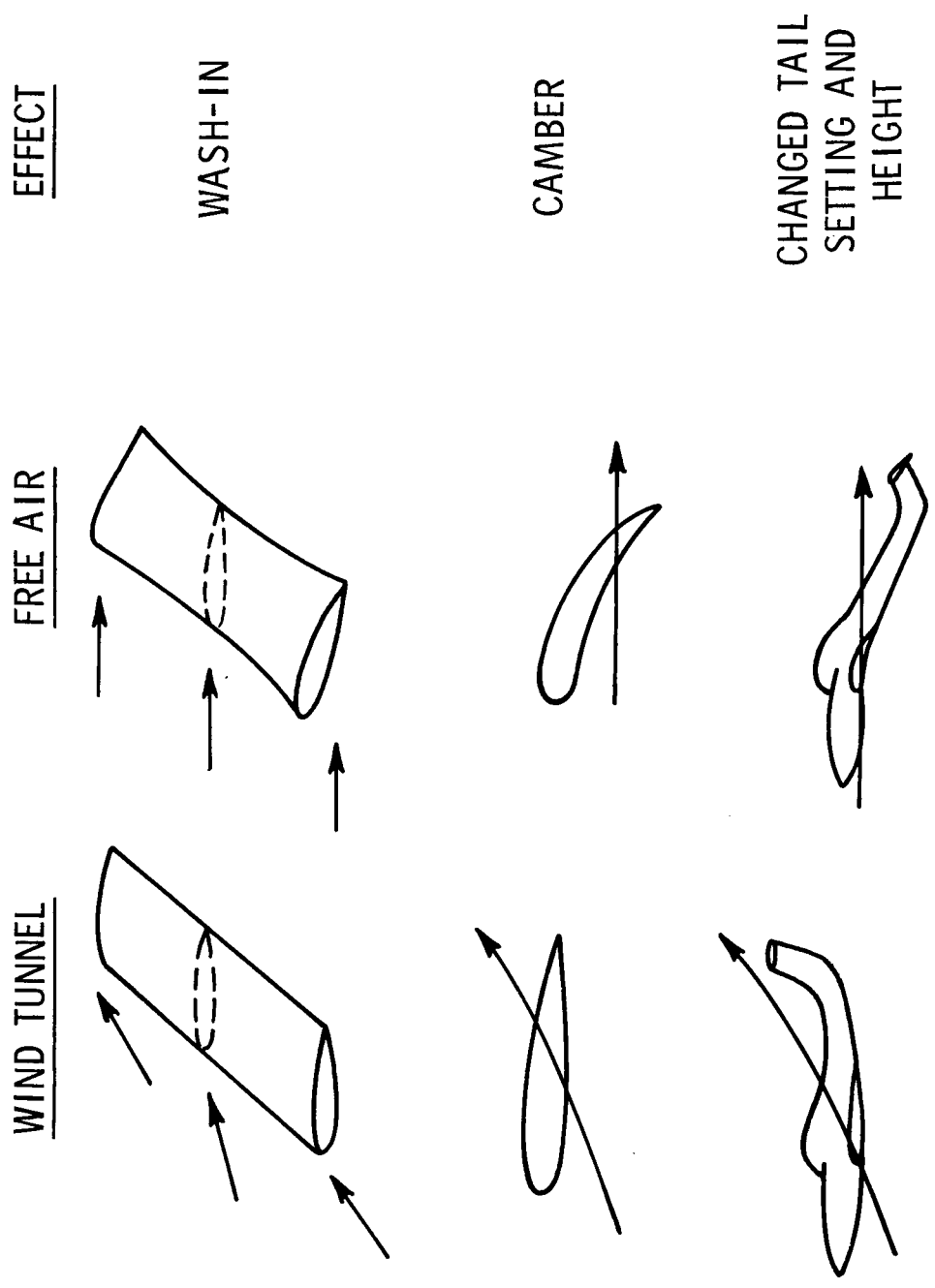


Figure 26.- Sketches illustrating the manner in which nonuniform interference can be considered as an equivalent effective aerodynamic distortion of the model.

# NONUNIFORM INTERFERENCE AS EFFECTIVE ROTATION

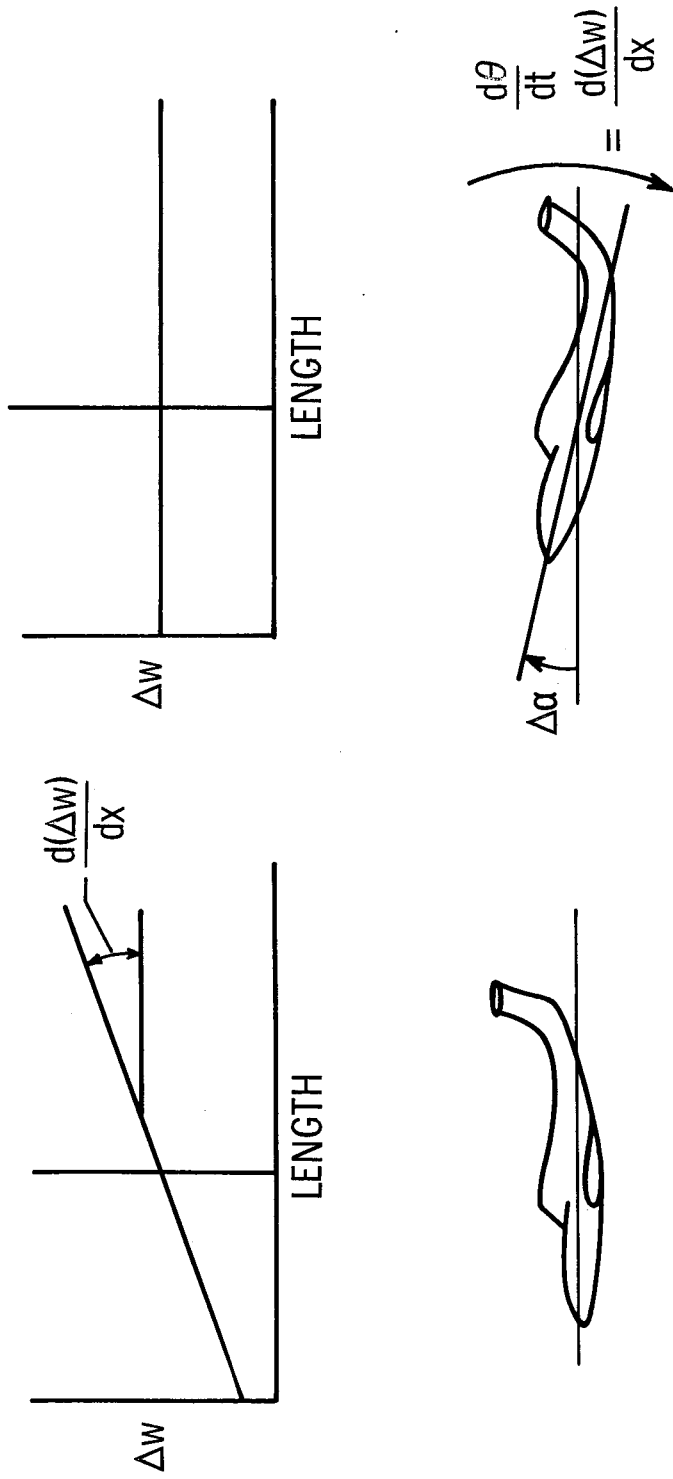
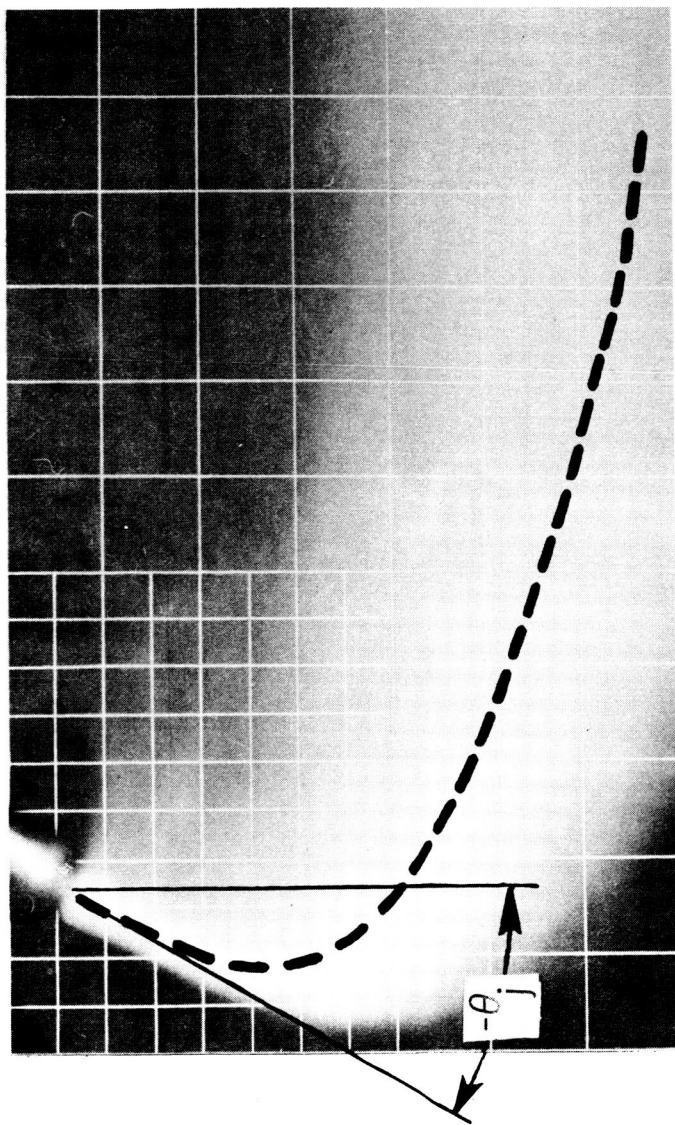


Figure 27.- Sketches illustrating the manner in which nonuniform interference can be considered as an equivalent effective aerodynamic rate of rotation.



$$\frac{x}{D} = \frac{1}{4} \left( \frac{V}{V_j} \right)^2 \left( \frac{-z}{D} \right)^3 \sec^2 \theta_j + \left( \frac{-z}{D} \right) \tan \theta_j$$

Figure 28.- The center-line path of jet wakes as obtained from flow visualization studies.

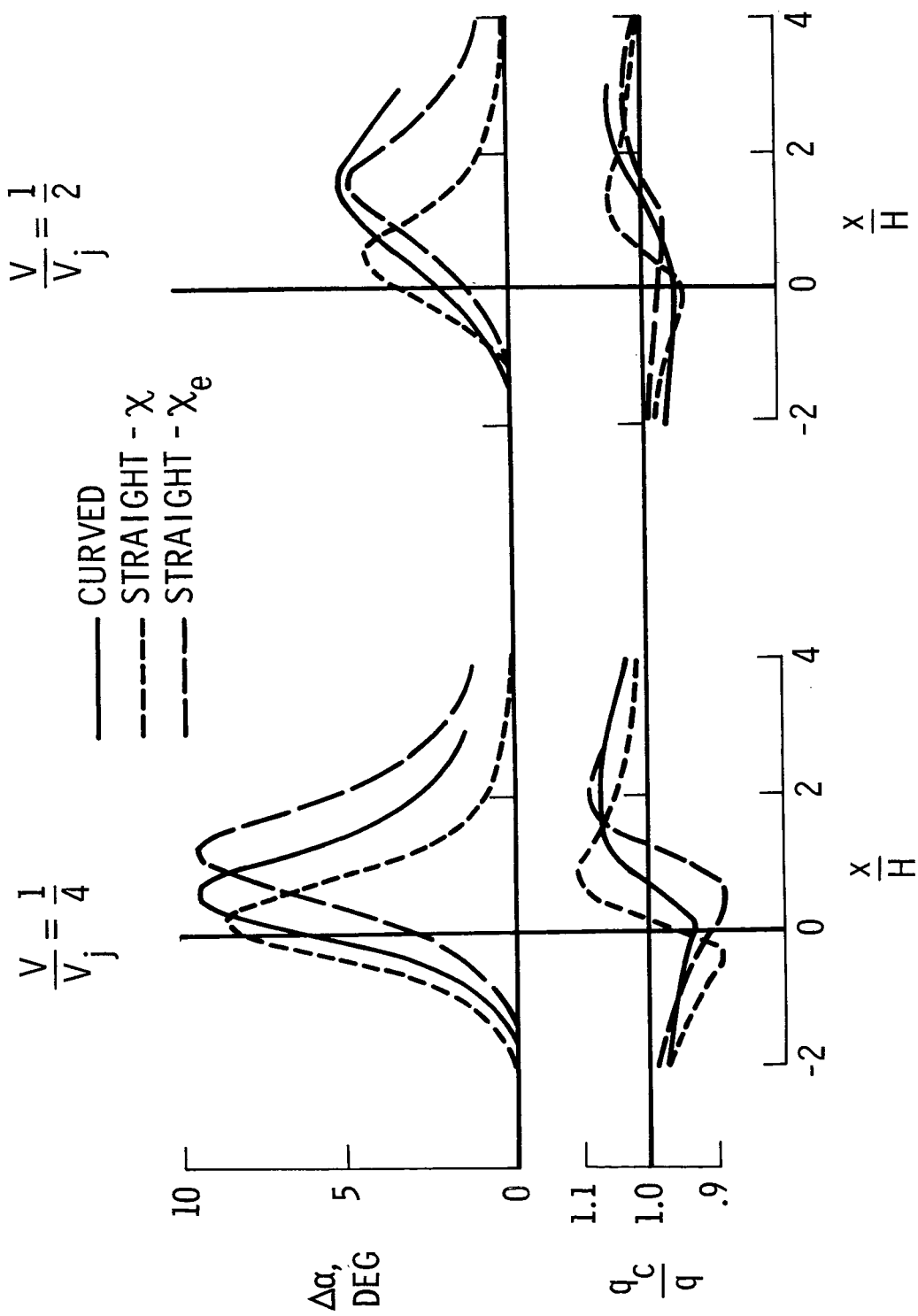


Figure 29.- Comparison of interference calculated with curved and straight wakes. Jet is centered in closed tunnel.  $\gamma = 1.5$ ,  $\theta_j = 0^\circ$ ,  $D = 0.4H$ .

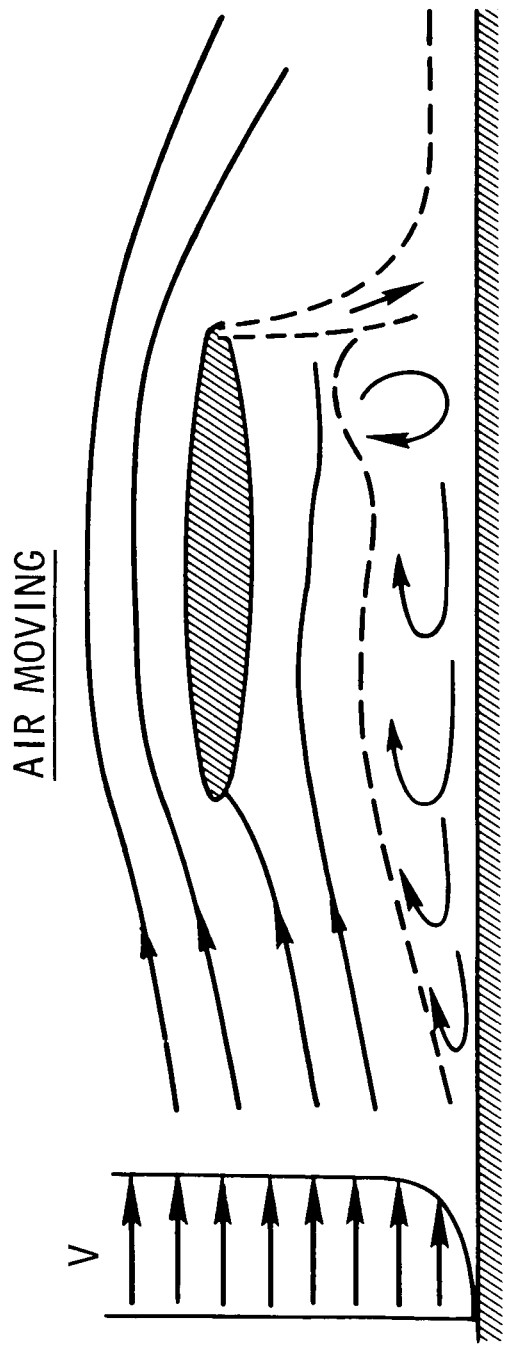
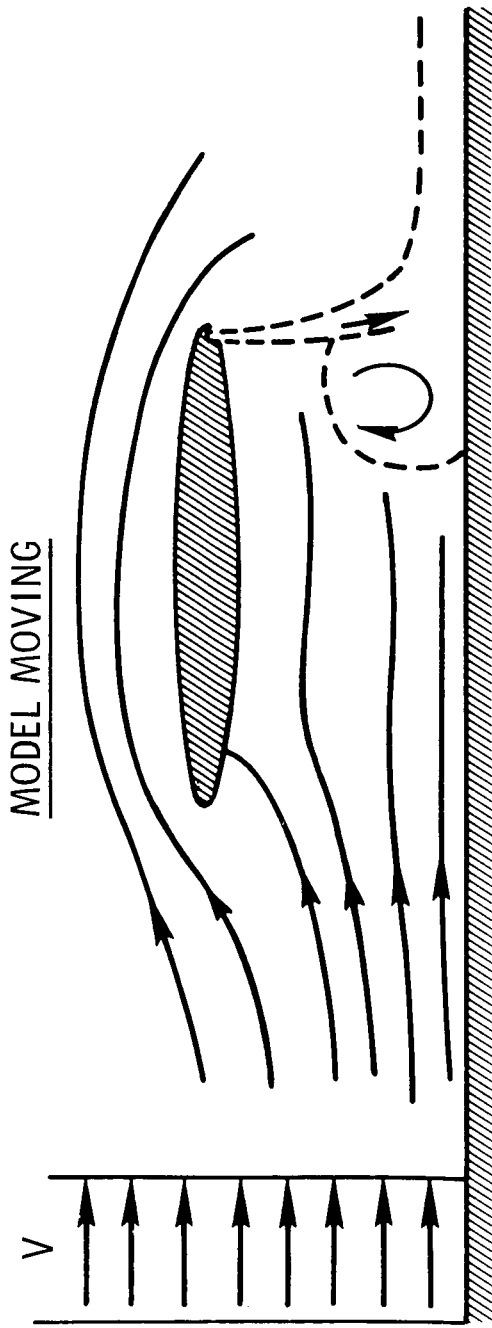


Figure 30.- Flow studies of a jet-flap wing operating near the ground.

# FULL-SPAN HIGH-LIFT CONFIGURATIONS

- DOUBLE SLOTTED FLAP,  $A = 10$
- JET FLAP,  $A = 6$
- ◇ TILT WING,  $A = 8.5$

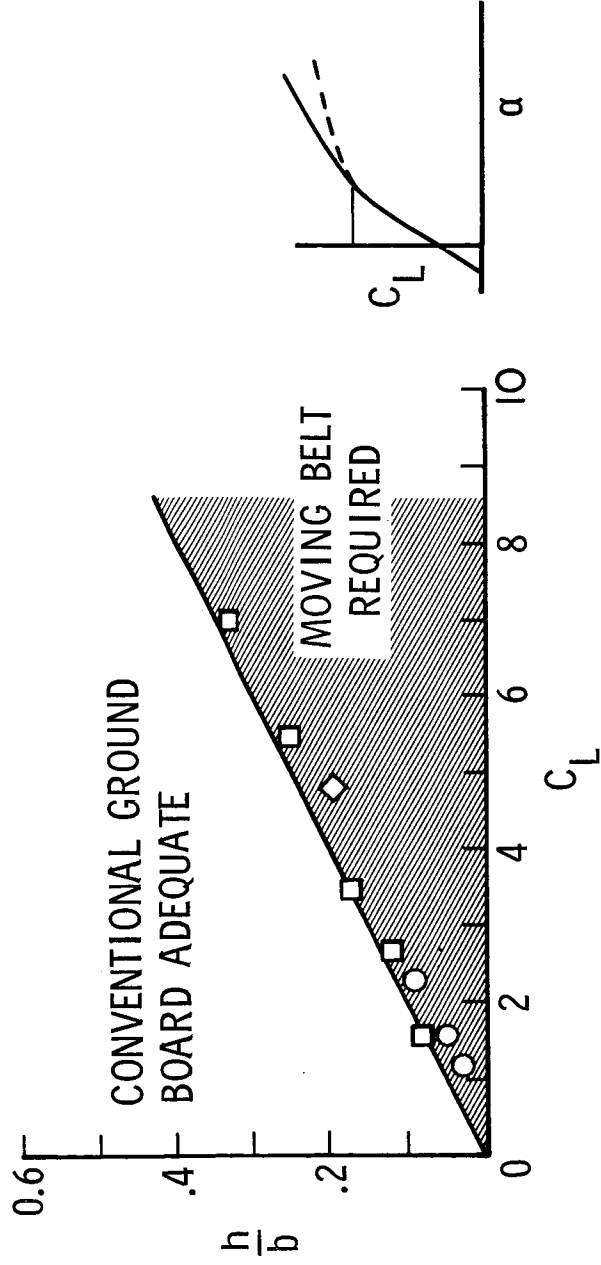


Figure 31.- Conditions which require the use of a moving belt when testing full-span high-lift configurations in ground effect.

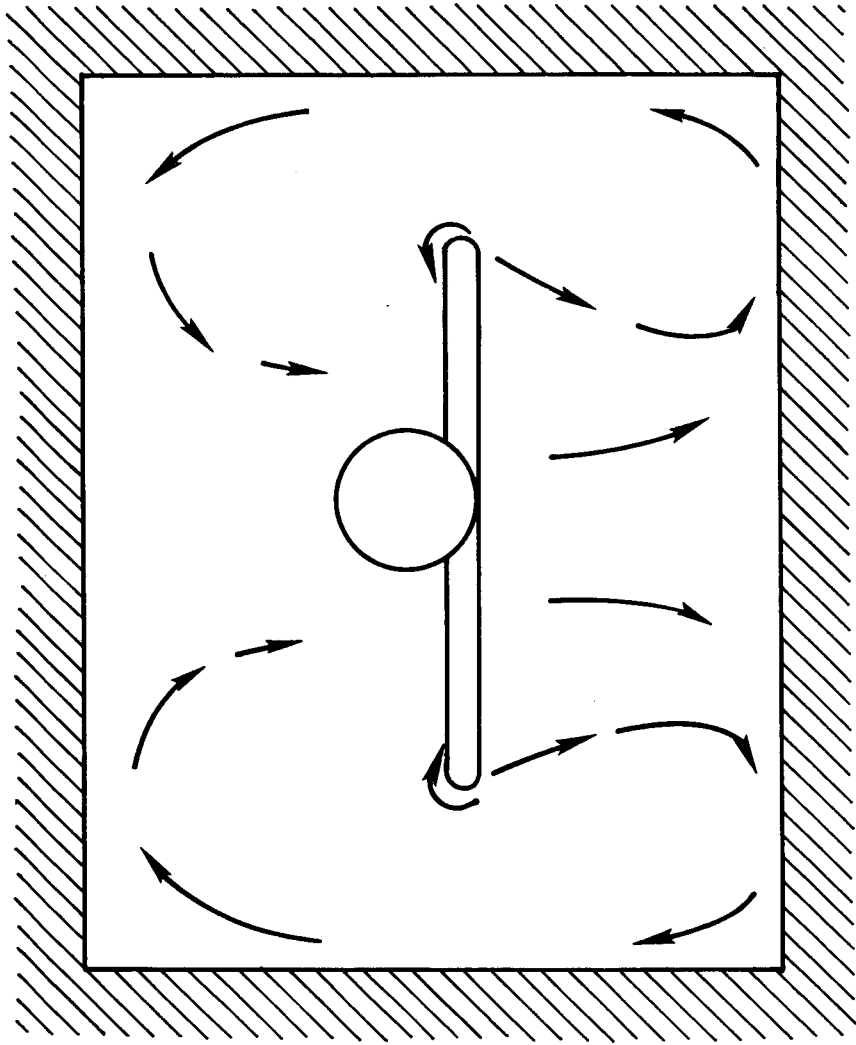


Figure 32.- Sketch illustrating the flow behind a lifting model in a closed wind tunnel.

# LATERAL RECIRCULATION LIMITS

- ROTOR
- TILT WING
- ◇ JET FLAP

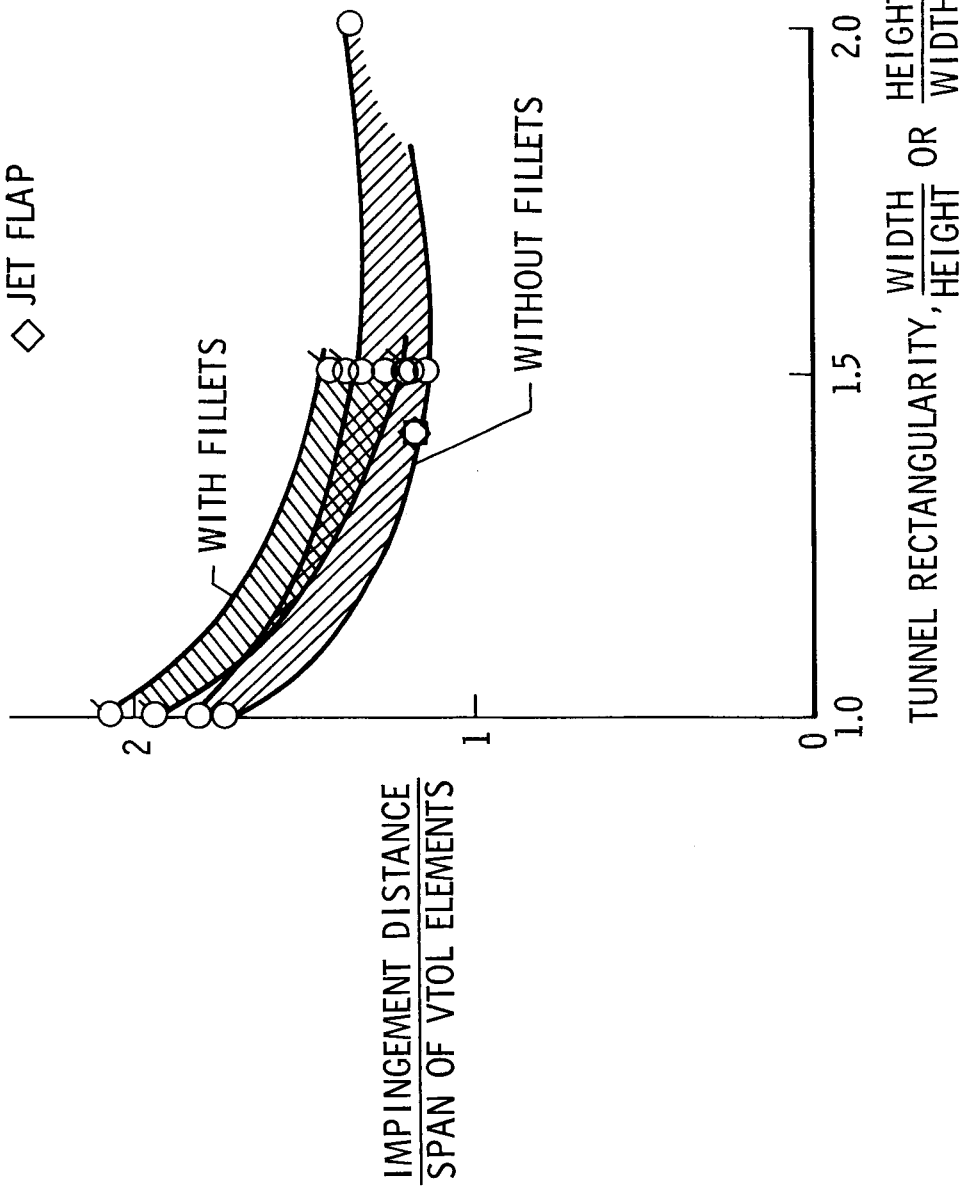


Figure 33.- Limits on maximum wake deflection when testing V/STOL models in closed wind tunnels.

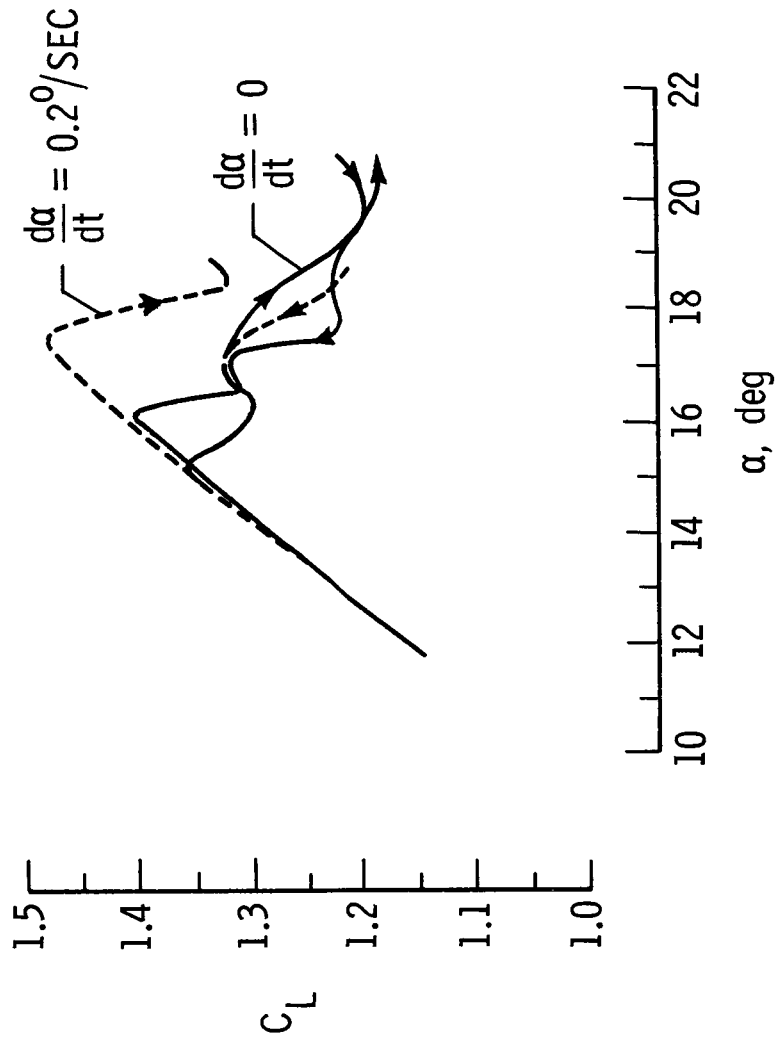


Figure 34.- Effect of rate-of-change of angle of attack on the lift curve of a monoplane near stall.